2. Physical Models

Solving the semiconductor equations is a difficult task in two ways. Not only are the semiconductor equations difficult to program on a computer, it is also difficult to formulate a complete mathematical model of semiconductor devices. The literature often presents models only in the broadest sense without a full explanation of the details. The general models in SimWindows are not new, but SimWindows incorporates many enhancements to those models. These enhancements allow SimWindows to simulate a greater range of devices, to increase the accuracy of simulations, and to extend the operating conditions applied to devices. This chapter describes the complete mathematical problem which SimWindows solves, and all the equations are in a continuous form. This chapter discusses concepts and equations that are readily available in the literature only briefly while explaining new extensions to the typical models in more detail.

This chapter contains six sections. Section 2.1 gives a complete list of symbols and their definitions. This chapter uses conventional symbols for most variables, but it will note any special variable or confusing nomenclature. Section 2.2 describes the statistics and transport of electrons and holes in semiconductor devices under equilibrium and non-equilibrium conditions. Only this portion of the model is necessary when simulating simple devices at a single constant (isothermal) temperature . Section 2.3 explains the photon portion of the model that SimWindows uses to simulate optical devices like laser diodes or solar cells. Section 2.4 describes the statistics and transport of the energy associated with electrons and holes. This additional portion of the model is necessary when simulating devices with a varying (non-isothermal)

temperature. These first four sections comprise the complete model that SimWindows solves.

One primary enhancement to the typical semiconductor models in SimWindows is the treatment of quantum wells. Many optoelectronic devices incorporate quantum wells into their structure, and SimWindows uses a scheme for modeling quantum wells. The various sections of this chapter describe the quantum well model along with their bulk counterparts. Section 2.5 will summarize the key aspects and discuss limitations of the quantum well model as a whole.

All of the semiconductor equations depend on a number of material parameters and operating conditions that the user supplies. Section 2.6 explains the wide variety of unknowns, that define materials, devices, and operating conditions.

This chapter presents a considerable number of equations. Five appendices summarize the results of this chapter. Appendix D repeats the list of symbols and their definitions. Appendix E gives a complete list of continuous equations from this chapter. Appendix F provides discrete forms of the important differential equations in Appendix E. Appendix G presents derivations of a few specific equations, and Appendix H details properties of important mathematical functions.

2.1 Nomenclature

The following sections list the symbols, definitions, and units of the fundamental variables that SimWindows solves, the specified variables that the user supplies, and the computed variables that SimWindows generates. The equations in this section do not consider different units, and there are no terms in the equations that are present simply to convert between units. For example, various equations interchange electron volts (eV) with Joules (J) without including an extra q to convert between electron volts and Joules.

2.1.1 Fundamental Variables

$f(x)$	Electrostatic Potential (V)
$h_c(x) = (E_{fn}(x) - E_c(x))/kT_n(x)$	Electron Planck potential (unitless)
$h_v(x) = (E_v(x) - E_{fp}(x))/kT_p(x)$	Hole Planck potential (unitless)
S	Total number of photons in a mode (unitless)
$T_L(x)$	Lattice Temperature (K)
$T_n(x)$	Electron Temperature (K)
$T_p(x)$	Hole Temperature (K)

2.1.2 Specified Variables

A_c	Area of a laser cavity (cm^2)
B	Spontaneous recombination constant ($cm^3\ s^{-1}$)
B_{qw}	QW spontaneous recombination constant ($cm^2\ s^{-1}$)
E_D,E_A	Donor and acceptor energy level relative to nearest band (eV)
E_g	Band Gap (eV)
g_D,g_A	Donor and acceptor degeneracy factor (unitless)
L	Total length of the device (cm)
L_c	Laser cavity length (cm)
L_{qw}	Length of the quantum well (cm)
m_n^*,m_p^*	Electron and hole density of states mass (kg)
m_{cn}^*,m_{cp}^*	Electron and hole conductivity mass (kg)
n_{real}	Real part of the refractive index (unitless)
N_D,N_A	Total donor and acceptor concentrations (cm^{-3})
r_d	Device radius (cm)
r_e	Environment radius (cm)
R_l, R_r	Reflectivities of left and right mirrors (unitless)

T_{env}	Environment temperature (K)
T_l, T_r	Temperature of left and right surfaces (K)
V_l, V_r	Bias of left and right contacts (V)
x	Position (cm)
a	Absorption coefficient (cm^{-1})
a_s	Laser scattering loss (cm^{-1})
b	Fraction of spontaneous photons emitted into lasing mode (unitless)
$\in$	Dielectric permitivity (F cm^{-1})
k	Thermal conductivity (J s^{-1} cm^{-1} K^{-1})
k_l, k_r	Thermal conductivities of the left and right surfaces (J s^{-1} cm^{-2} K^{-1})
m_n, m_p	Electron and hole mobilities (cm^2 V^{-1} s^{-1})
u_n,u_n	Power dependence of the electron and hole momentum relaxation times (unitless)
u_{opt}	External optical generation frequency (s^{-1})
t_n, t_n	Electron and hole shr recombination lifetime (s)
t_{wn}, t_{wn}	Electron and hole energy relaxation lifetime (s)
c	Electron affinity (eV)

2.1.3 Computed Variables

$A^*_{n,p}$	Electron and hole Richardson constants (A cm^{-2} K^{-2})
$\mathbf{D}$	Electrostatic Displacement (C cm^{-2})
$\mathcal{E}$	Electrostatic field (V cm^{-1})
$\mathcal{E}_{stim}$	Normalized stimulated electromagnetic field ($cm^{-3/2}$)
E_c, E_v	Conduction and valence band edges (eV)
$E_{c,top}$,$E_{v,top}$	Conduction and valence band energies of the top of a QW (eV)
E_{fn}, E_{fp}	Electron and hole quasi-fermi levels (eV)
E_{gqw}	Quantum well band gap (bulk band gap plus electron and hole quantized energy levels) (eV)
E_j^+, E_j^-	Forward and reverse propagating electric fields (unitless)
$E_{n,stim}$, $E_{p,stim}$	Electron and hole stimulated emission energies (eV)
E_{qwn},E_{qwp}	Electron and hole QW quantized energy level (eV)
g	Local gain (cm^{-1})
G_{opt}	Total external optical generation rate (cm^{-3} s^{-1})
$G_{u\,opt}$	External optical generation rate at a specific frequency (cm^{-3} s^{-1})
$\mathbf{J}_n$, $\mathbf{J}_p$	Electron and hole current density (A cm^{-2})
$\mathbf{J}^{therm}_{n,p\longrightarrow+}$, $\mathbf{J}^{therm}_{n,p+\rightarrow-}$	Electron and hole current due to thermionic emission traveling from left to right (- to +) and right to left (+ to -) (A cm^{-2})
$\mathbf{J}^{tun}_{n,p\longrightarrow+}$, $\mathbf{J}^{tun}_{n,p+\rightarrow-}$	Electron and hole current due to tunneling traveling from left to right (- to +) and right to left (+ to -) (A cm^{-2})
k_o	Free space wave vector (cm^{-1})

m_{qwn}^{*}, m_{qwp}^{*}	Electron and hole DOS masses in a quantum well (kg)
$m_{bulkn}^{*}, m_{bulkp}^{*}$	Electron and hole DOS masses in bulk material (kg)
n, p	Total electron and hole concentration (cm^{-3})
n_b, p_b	QW bound electron and hole concentration (cm^{-3})
n_f, p_f	QW free electron and hole concentration (cm^{-3})
n_i	Bulk intrinsic carrier concentration (cm^{-3})
$n_{i,2d}$	QW intrinsic carrier concentration (cm^{-3})
n_j	Complex refractive index of region j (unitless)
n_{2d}, p_{2d}	Total QW electron and hole concentration (cm^{-2})
N_c, N_v	Effective conduction and valence bands density of states (cm^{-3})
N_{cqw}, N_{vqw}	Effective quantum well conduction and valence bands density of states (cm^{-2})
N_D^+, N_A^-	Ionized donors and acceptor concentrations (cm^{-3})
$\langle S_j \rangle$	Total Poynting vector for a propagating electromagnetic field (W cm^{-2})
$\langle S_j^+ \rangle, \langle S_j^- \rangle$	Time averaged Poynting vectors for forward and reverse propagating electromagnetic fields (W cm^{-2})
$\mathbf{S}_n^{tot}, \mathbf{S}_p^{tot}$	Electron and hole total energy flow (J cm^{-2} s^{-1})
$\mathbf{S}_{n,p}^{therm}$	Electron and hole total energy flow due to thermionic emission (J cm^{-2} s^{-1})
$\mathbf{S}_{n,p-\rightarrow+}^{therm}, \mathbf{S}_{n,p+\rightarrow-}^{therm}$	Electron and hole kinetic energy flow due to thermionic emission traveling from left to right (- to +) and right to left (+ to -) (J cm^{-2} s^{-1})
$\mathbf{S}_{n,p}^{tun}$	Electron and hole total energy flow due to tunneling (J cm^{-2} s^{-1})
$\mathbf{S}_{n,p-\rightarrow+}^{tun}, \mathbf{S}_{n,p+\rightarrow-}^{tun}$	Electron and hole kinetic energy flow due to tunneling traveling from left to right (- to +) and right to left (+ to -) (J cm^{-2} s^{-1})
$\mathbf{S}_{lat}$	Lattice energy flow (J cm^{-2} s^{-1})
$U_{c-,v-}, U_{c+,v+}$	Conduction and valence barrier heights seen from the left (-) and the right (+) (eV)
U_{tot}	Total carrier recombination rate (cm^{-3} s^{-1})
$U_{stim}, U_{b\text{-}b}, U_{shr}$	Stimulated, Band to band, and Shockley-Hall-Reed recombination (cm^{-3} s^{-1})
$\tilde{U}_{stim}, \tilde{U}_{b-b}$	Total stimulated and spontaneous recombination rates in the laser cavity (s^{-1})
u_n, u_p	Total electron and hole energy density (J cm^{-3})
$u_{n,2d}, u_{p,2d}$	Total QW electron and hole energy density (J cm^{-2})
V_{qwn}, V_{qwp}	Conduction and Valence QW heights (eV)
v_{stim}	Velocity of stimulated emission photons (cm s^{-1})
W_n^{tot}, W_p^{tot}	Total electron and hole energy loss rate (J cm^{-3} s^{-1})
$W_{n,shr}^{tot}, W_{p,shr}^{tot}$	Total electron and hole SHR energy loss (J cm^{-3} s^{-1})

$W_{n,b-b}^{tot}, W_{p,b-b}^{tot}$	Total electron and hole spontaneous energy loss (J cm^{-3} s^{-1})
$W_{n,stim}^{tot}, W_{p,stim}^{tot}$	Total electron and hole stimulated energy loss (J cm^{-3} s^{-1})
$W_{n,opt}^{tot}, W_{p,opt}^{tot}$	Total electron and hole external optical energy loss (J cm^{-3} s^{-1})
$W_{n,relax}^{tot}, W_{p,relax}^{tot}$	Total electron and hole relaxation energy loss (J cm^{-3} s^{-1})
W_{lat}^{tot}	Total lattice energy loss (J cm^{-3} s^{-1})
Z_j	relative complex impedance in region j (unitless).
a_m	Distributed mirror loss (cm^{-1})
f_0	Built-in Potential (V)
h_{c0}, h_{v0}	Charge neutral values of the electron and hole Planck potentials (eV)
k_e	Effective environment thermal conductivity (J cm^{-1} K^{-1})
u_{stim}	Stimulated emission frequency (s^{-1})
r	Total Charge (C cm^{-3})
y_n, y_p	Electron and hole QW wavefunction (cm$^{-1/2}$)
t_{ph}	Photon lifetime (s)

2.1.4 Constants

q - Electronic charge (1.602 x 10^{-19} C)
k - Boltzmann Constant (8.62 x 10^{-5} eV K^{-1})
h - Planck Constant (6.626 x 10^{-34} J s)
$\hbar$ - Planck Constant/2p (1.0546 x 10^{-34} J s)
i - (-1)$^{0.5}$
p - Pi (3.141592654)

2.2 Charge

Any semiconductor device simulator must solve the equations describing the statistics and transport of charge through the device under equilibrium and non-equilibrium conditions. Three fundamental variables are necessary to describe uniquely the charge in a semiconductor device. Fundamental variables are variables that, once solved, can yield all other unknowns. In theory, the choice of variables is arbitrary, but it is easier numerically to solve variables that do not change by orders of magnitude over the length of the device. The variables chosen here are the electrostatic potential, $f(x)$, the electron Planck potential, $h_c(x)$, and the hole Planck potential, $h_v(x)$ [7]. The

expressions relating the Planck potentials to the quasi-fermi levels and band edges are:

$$h_c(x) = (E_{fn}(x) - E_c(x))/kT_n(x) \tag{1}$$

$$h_v(x) = (E_v(x) - E_{fp}(x))/kT_p(x) \tag{2}$$

Three equations are necessary to solve the three fundamental variables. These equations vary depending on the simulation type: either equilibrium or non-equilibrium. In addition to equilibrium and non-equilibrium states, a third state, charge-neutral, is also useful to calculate. This is a non-physical state that SimWindows calculates prior to solving the equilibrium and non-equilibrium states.

There are a few equations that are common to each of the three states of a device. These are the effective density of states, the total carrier concentrations, the ionized doping concentrations, and the total charge. The bulk versions of these equations are:

$$N_{c,v}(x) = \frac{1}{4p^{\frac{3}{2}}}\left(\frac{2m^*_{n,p}(x)kT_{n,p}(x)}{\hbar^2}\right)^{\frac{3}{2}} \tag{3}$$

$$n(x) = N_c F_{1/2}(h_c) \qquad p(x) = N_v F_{1/2}(h_v) \tag{4}$$

$$N_D^+(h_c) = \frac{N_D}{1 + g_D e^{E_D/kT_n + h_c}} \qquad N_A^+(h_v) = \frac{N_A}{1 + g_A e^{E_A/kT_p + h_v}} \tag{5}$$

$$r(x) = q(p(x) - n(x) + N_D^+(x) - N_A^-(x)) \tag{6}$$

where $F_j(x)$ is the Fermi integral of order j (see Appendix H).

Equations (3) and (4) are different for quantum wells due to the two-dimensional density of states in a quantum well. SimWindows uses a model for the charge in the quantum well that incorporates both the bound charge and the free

charge. The density of states diagram in Figure 3 shows the distinction between these two types of charge. This model is similar in concept to the model presented in [13], but it uses some slightly different assumptions which lead to different expressions.

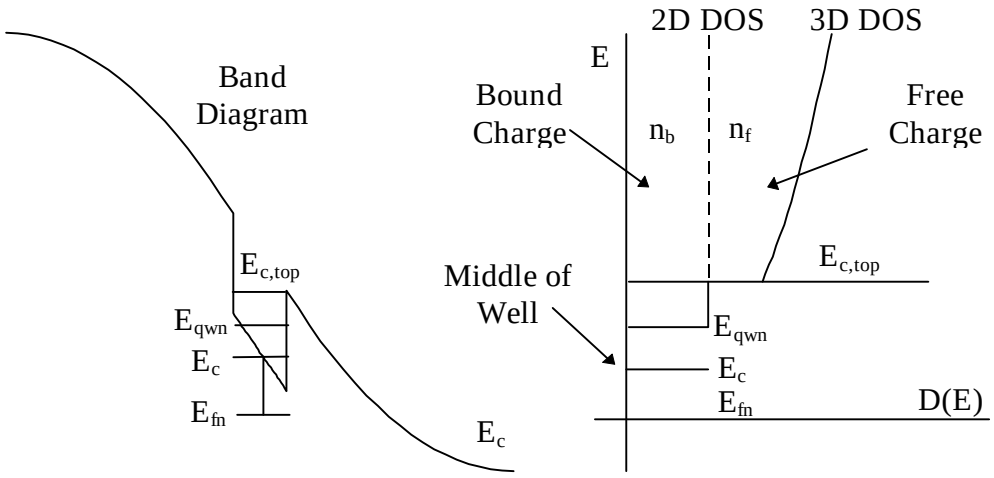

Figure 3 - Quantum well and corresponding density of states

The equations for the total charge in a quantum well employ several assumptions. 1) There is only one bound state below $E_{c,top}$, all states above $E_{c,top}$ are free. 2) The quantized energy level, E_{qwn}, is constant relative to the conduction band at the middle of the quantum well. 3) There is an abrupt transition between the two-dimensional and the three-dimensional density of states at an energy of $E_{c,top}$. 4) The quasi-fermi level is constant in the well. 5) Boltzmann statistics can describe the free charge. Using these assumptions, the equations for the bound carrier concentrations are:

$$N_{c,vqw} = \frac{m^*_{n,p} k T_{n,p}}{p\hbar^2} \tag{7}$$

$$n_{2d} = N_{cqw} F_0\left(h_c - \frac{E_{qwn}}{kT_n}\right) \qquad p_{2d} = N_{vqw} F_0\left(h_v - \frac{E_{qwp}}{kT_p}\right) \tag{8}$$

$$n_b(x) = |y_{n}(x)|^2 n_{2d} \qquad p_b(x) = |y_{p}(x)|^2 p_{2d} \tag{9}$$

The equations for the free carrier concentrations are (see Derivation 1 in Appendix G):

$$n_f(x) = e^{h_c}\left[N_c(x)\left(1 - \frac{g(\frac{3}{2}, \frac{E_{c,top}}{kT_n})}{\sqrt{p}/2}\right) - \frac{N_{cqw}}{L_{qw}} e^{-\frac{E_{c,top}}{kT_n}} \right] \tag{10}$$

$$p_f(x) = e^{h_v}\left[N_v(x)\left(1 - \frac{g(\frac{3}{2}, \frac{E_{v,top}}{kT_p})}{\sqrt{p}/2}\right) - \frac{N_{vqw}}{L_{qw}} e^{-\frac{E_{v,top}}{kT_p}} \right] \tag{11}$$

where $\gamma(3/2,x)$ is the incomplete gamma function of order 3/2 (see Appendix H). The total carrier concentration is just the sum of the bound (9) and free carrier concentrations (10,11). Note that the units on the bound and free carrier concentrations are in cm^{-3} which is necessary for these equations to be compatible with the total charge (6).

The quantum well carrier concentration equations depend both on the quantized energy levels and wavefunctions in the quantum well. SimWindows uses the finite square well solution to Schrödinger's equation for the energy level and the infinite square well solution for the wavefunction. These equations are:

$$\sqrt{\frac{2m^*_{qwn,p}E_{qwn,p}}{\hbar^2}}\tan\left(\sqrt{\frac{2m^*_{qwn,p}E_{qwn,p}}{\hbar^2}}\frac{L_{qw}}{2}\right) - \sqrt{\frac{2m^*_{bulkn,p}\left(V_{qwn,p} - E_{qwn,p}\right)}{\hbar^2}} = 0 \tag{12}$$

$$y_{n,p}(x) = \sqrt{\frac{2}{L_{qw}}}\sin\left(\frac{px}{L_{qw}}\right) \tag{13}$$

2.2.1 Charge-neutral

Charge neutrality is a non-physical device state in which there is no net charge at all points in the device. SimWindows uses it only as a starting point for more simulations. It calculates the electrostatic potential and the electron and hole Planck

potentials under the assumption of no net charge. All of the three main equations are simple algebraic equations, which makes solving them a relatively simple problem. The main equations for charge neutrality are:

$$p(-h_{c0} - E_g/kT_L) - n(h_{c0}) + N_D^+(h_{c0}) - N_A^-(-h_{c0} - E_g/kT_L) = 0 \qquad (14)$$

$$f(x) = -kT_L h_{c0}(0) + c(0) - c(x) + kT_L h_{c0}(x) \qquad (15)$$

$$h_{v0}(x) = -h_{c0}(x) - E_g(x)/kT_L \qquad (16)$$

In the most general case, equation (14) does not have an analytical solution for the electron Planck potential. However, under the assumptions that Boltzmann statistics is valid (a fermi integral approaches an exponential) and complete ionization (Nd^+=Nd and Na^+=Na), there are analytical solutions for h_{c0}, h_{v0}, and f. Depending on the options that the user selects, SimWindows solves equation (14) either numerically or analytically. Equations (14) through (16) also imply that the electron and hole quasi-fermi levels are constant and at the same energy.

From the results of the charge neutral calculations, SimWindows calculates two other values that other calculations use. The first is the built in potential which SimWindows finds by evaluating (15) at a position equal to the length of the device, L.

$$f_0 = -kT_L h_{c0}(0) + c(0) - c(L) + kT_L h_{c0}(L) \qquad (17)$$

The second is the intrinsic carrier concentration which is the product of the electron and hole concentrations when the material is in equilibrium. For bulk materials, the intrinsic carrier concentration is:

$$n_i^2 = N_c(T_L) N_v(T_L) e^{-E_g/kT_L} \frac{F_{1/2}(h_{c0})}{e^{h_{c0}}} \frac{F_{1/2}(h_{v0})}{e^{h_{v0}}} \qquad (18)$$

For quantum wells, the expression for the intrinsic carrier concentration is:

$$n_{i,2d}^2 = N_{cqw}(T_L)N_{vqw}(T_L)e^{-E_{gqw}/kT_L}\frac{F_0\left(h_{c0}-\frac{E_{qwn}}{kT_L}\right)}{e^{h_{c0}-\frac{E_{qwn}}{kT_L}}}\frac{F_0\left(h_{v0}-\frac{E_{qwp}}{kT_L}\right)}{e^{h_{v0}-\frac{E_{qwp}}{kT_L}}} \tag{19}$$

2.2.2 Equilibrium

Equilibrium differs from charge neutrality since there can be a net charge at specific locations in the device but not in the device as a whole. Electron and hole quasi-fermi levels are still constant and equal. The three main equations that SimWindows solves under equilibrium conditions are:

$$\nabla \bullet \mathbf{D}(x) - r(x) = 0 \tag{20}$$

$$h_c(x) = \frac{f(x) + c(x) - c(0)}{kT_L} + h_c(0) \tag{21}$$

$$h_v(x) = -h_c(x) - E_g(x)/kT_L \tag{22}$$

Of the three main equations, only Poisson's equation (20) is a differential equation. This is a more difficult problem to solve than the charge-neutral case, but numerical methods can solve the equation quickly. Equation (20) also requires an equation for the electrostatic displacement, **D**:

$$\mathbf{D}(x) = -\in(x)\nabla f(x) \tag{23}$$

2.2.3 Non-equilibrium

The main characteristic of non-equilibrium is that external means, for example an applied bias or incident light, generate or deplete carriers to produce a net recombination/generation rate. This gives rise to a current. This is the most general and useful situation, but it is considerably more difficult to solve since it involves three differential equations for the potential and the electron and hole Planck potentials. The

next three sections discuss the important rate equations, the current equations, and the various recombination and generation processes.

2.2.3.1 Rate Equations

A device under non-equilibrium conditions requires three electrical equations to solve. These are Poisson's equation (24) and the two current continuity equations (25,26). SimWindows presently implements (25) and (26) only in steady state, in which case the time derivatives are zero.

$$\nabla \bullet \mathbf{D}(x) - r(x) = 0 \tag{24}$$

$$\nabla \bullet (\mathbf{J_n}(x)/q) - U_{tot}(x) = \frac{\partial n}{\partial t} \tag{25}$$

$$\nabla \bullet (\mathbf{J_p}(x)/q) + U_{tot}(x) = -\frac{\partial p}{\partial t} \tag{26}$$

As with the equilibrium case, Poisson's equation still requires (23) as an auxiliary equation. The two continuity equations require auxiliary relations for the current and the net recombination rate.

2.2.3.2 Current

Current is nothing more than the flow of carriers from one location to another. However, a variety of relationships can describe current depending on the nature of the current. The fundamental method for determining the electron current is to evaluate the following integral:

$$\mathbf{J}_n = \frac{-q}{4\pi^3} \iiint \mathbf{v} f dk_x dk_y dk_z \tag{27}$$

This equation expresses the electron current as the integral of the velocity of the carriers, **v**, times the distribution of the carriers, *f*, over all momentum. The

expression for hole current is the same except a positive charge is used instead of a negative charge.

SimWindows implements three common types of current: drift-diffusion, thermionic emission, and tunneling. It applies drift-diffusion in devices of a single material or gradually graded materials. It uses thermionic emission between a quantum-well and a bulk material. It uses thermionic emission and tunneling currents at abrupt boundaries between two bulk materials. To determine the distinction between a gradually graded material and an abrupt heterojunction, SimWindows uses the criteria [14]:

$$\frac{2kT_{n,p}l_g}{\Delta E_{c,v}} < l_m \tag{28}$$

where l_g is the length of the grading region, l_m is the mean free path of the carrier, and $\Delta E_{c,v}$ is the change in the band edge. If the grading region is short enough to satisfy (28), then the carriers will not undergo any collisions in the grading layer. In this case SimWindows uses the thermionic emission and tunneling current expressions. If the grading region does not satisfy (28) then it uses the drift-diffusion current expressions.

2.2.3.2.1 Drift Diffusion

Drift-diffusion current arises from an external force applied to the carriers. As a result, the energy distribution of the carriers in (27) is different from the equilibrium Fermi-Dirac distribution. The derivation for the drift-diffusion current [15,16] assumes the non-equilibrium distribution is the sum of the equilibrium distribution plus a small perturbation. The relaxation time approximation to the Boltzmann transport equation yields a result for the perturbation, f_1:

$$f_1 = -t\left(\mathbf{v} \bullet \nabla_r f_0 + \frac{\mathbf{F}}{\hbar} \bullet \nabla_k f_0\right) \tag{29}$$

where t is the momentum relaxation time, and **F** is the force on the carrier. The momentum relaxation time is dependent on the energy of the carrier with the dominant scattering mechanism determining the energy dependence. By using a simple power law to describe the energy dependence of the momentum relaxation time:

$$t = t_0\left(E - E_c\right)^{u_{n,p}} \tag{30}$$

the user can choose a $u_{n,p}$ to correspond to the dominant scattering mechanism of the material. Using (29) and (30), equation (27) yields [15]:

$$\mathbf{J}_n = \frac{q t_0}{4p^3} \iiint \mathbf{v}\left(E - E_c\right)^{v_n}\left(\mathbf{v} \bullet \nabla_r f_0 + \frac{\mathbf{F}}{\hbar} \bullet \nabla_k f_0\right) dk_x dk_y dk_z \tag{31}$$

Evaluating (31) yields the drift-diffusion current equations:

$$\mathbf{J}_n = m_n n\left\{\left(kT_n \nabla h_c + \nabla E_c\right) + \left(\tfrac{5}{2} + u_n\right)\frac{F_{3/2+u_n}(h_c)}{F_{1/2+u_n}(h_c)} \nabla kT_n\right\} \tag{32}$$

$$\mathbf{J}_p = -m_p p\left\{\left(kT_p \nabla h_v - \nabla E_v\right) + \left(\tfrac{5}{2} + u_p\right)\frac{F_{3/2+u_p}(h_v)}{F_{1/2+u_p}(h_v)} \nabla kT_p\right\} \tag{33}$$

These equations are not the standard equations that the literature often presents. However, equations (32) and (33) contain all of the physics necessary for device simulations. They apply to non-isothermal conditions as well as Fermi-Dirac statistics and graded material parameters. The user can also select the appropriate value for $u_{n,p}$ corresponding to the dominant carrier scattering mechanism for the material. By using:

$$\nabla h_{c,v} = \frac{F_{1/2}\left(h_{c,v}\right)}{F_{-1/2}\left(h_{c,v}\right)}\left(\frac{1}{n,p}\nabla n, p - \frac{3}{2}\frac{1}{T_{n,p}}\nabla T_{n,p} - \frac{3}{2}\nabla \ln\left(m^*_{n,p}\right)\right) \tag{34}$$

equations (32) and (33) yield the more typical drift-diffusion equations [17]:

$$\mathbf{J}_n = m_n kT_n \frac{F_{1/2}(h_c)}{F_{-1/2}(h_c)} \nabla n + m_n n \nabla E_c - \frac{3kT_n}{2} m_n \frac{F_{1/2}(h_c)}{F_{-1/2}(h_c)} n \nabla \ln(m_n^*) + m_n n \left(\left(\frac{5}{2} + u_n \right) \frac{F_{3/2+u_n}(h_c)}{F_{1/2+u_n}(h_c)} - \frac{3}{2} \frac{F_{1/2}(h_c)}{F_{-1/2}(h_c)} \right) \nabla kT_n \tag{35}$$

$$\mathbf{J}_p = -m_p kT_p \frac{F_{1/2}(h_v)}{F_{-1/2}(h_v)} \nabla p + m_p p \nabla E_v + \frac{3kT_p}{2} m_p \frac{F_{1/2}(h_v)}{F_{-1/2}(h_v)} p \nabla \ln(m_p^*) - m_p p \left(\left(\frac{5}{2} + u_p \right) \frac{F_{3/2+u_p}(h_v)}{F_{1/2+u_p}(h_v)} - \frac{3}{2} \frac{F_{1/2}(h_v)}{F_{-1/2}(h_v)} \right) \nabla kT_p \tag{36}$$

These equations relate current to the gradients of the carrier concentration, the band edge, the mass (resulting from the varying density of states), and the carrier temperature.

2.2.3.2.2 Thermionic Emission and Tunneling

Thermionic emission and tunneling currents apply when there is an abrupt change in either the conduction or valence band edges which forms a barrier to carrier flow. The derivation for the thermionic emission current assumes that all of the carriers with an energy above the top of the barrier contribute to the current. A similar derivation for the tunneling current assumes that only a fraction of the carriers with energy below the top of the barrier may tunnel through the barrier and contribute to the current. These derivations using Boltzmann statistics appear in [18], but the discussion below applies for Fermi-Dirac statistics. Figure 4 shows a barrier typically found in n-type DBR structures that use a thin AlGaAs region between adjacent GaAs and AlAs regions. Figure 4 also shows the carriers contributing to the current.

Evaluating the following integral will yield the electron current resulting from electrons emitted from the left side to the right side of the barrier:

$$\mathbf{J}_{n\to+} = -q\int_0^{\infty} \mathbf{v}_x T_n(E)\, g(E)\, f(E)\, dE \tag{37}$$

where $\mathbf{v}_x$ is the velocity of the carriers in the direction towards the barrier, $T_n(E)$ is the transmission probability over or through the barrier, $g(E)$ is the density of states, and $f(E)$ is the distribution function.

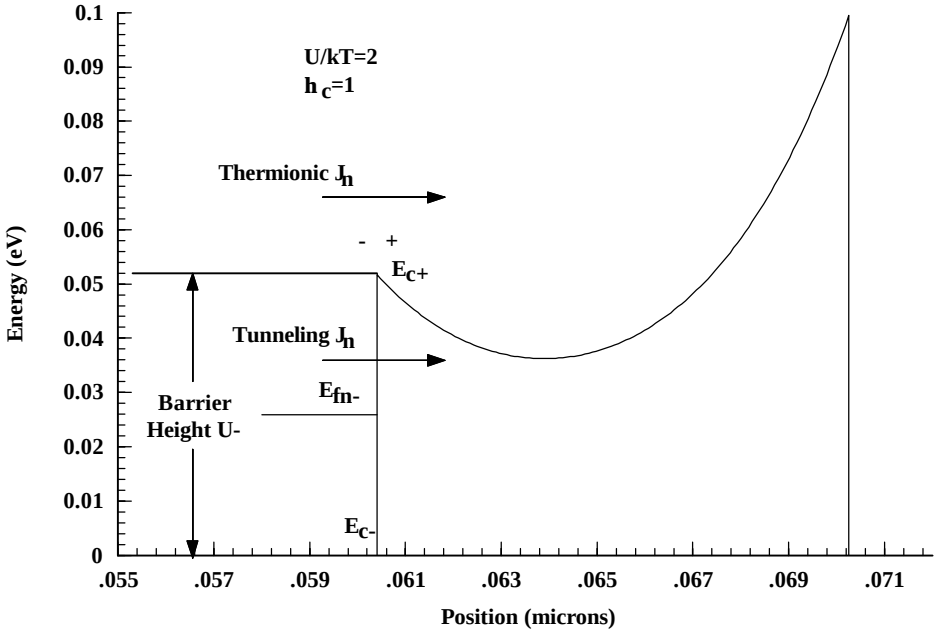

Figure 4 - Thermionic emission diagram

A similar integral applies for the carriers on the other side of the barrier, and the total current is just the difference between the two. Equation (37) can be split into two integrals representing the thermionic emission component and the tunneling component:

$$\mathbf{J}_{n\to+} = \underbrace{-q\int_{U_{c-}}^{\infty} \mathbf{v}_x g(E)\, f(E)\, dE}_{\text{Thermionic Emission}} \underbrace{-q\int_0^{U_{c-}} \mathbf{v}_x T_n(E)\, g(E)\, f(E)\, dE}_{\text{Tunneling}} \tag{38}$$

This equation assumes that the transmission probability is one for all thermionically emitted carriers. This is not exactly true since quantum mechanical calculations result in a transmission probability that is less than one for carriers both above and below the top of the barrier. To evaluate the transmission probability for carriers with energy less than the barrier, SimWindows uses the WKB approximation [19]:

$$T_n(E) = e^{-\frac{2p}{h}\int_0^{L(E)}\sqrt{2m^*(E_c - E)}dx} \tag{39}$$

Figure 5 shows the transmission probability versus energy for the barrier shown in Figure 4. The vertical lines denote the electron quasi-fermi level and the conduction band edge. These are located at the same energy in Figure 5 as the levels in Figure 4. The discontinuity in the transmission probability at 1.4 results from the local minimum in the conduction at 0.064 microns in Figure 4. For energies below this minimum, the tunneling probability reduces sharply because of the longer tunneling distance.

The first step in evaluating (38) is to split the energy terms into parallel (yz) and perpendicular (x) kinetic energy components. The parallel component corresponds to the motion of carriers parallel to the barrier interface, and the perpendicular component corresponds to the motion of carriers perpendicular to the barrier. It is the perpendicular component that contributes to the current. The split in the energy terms converts (38) into a double integral over the parallel and perpendicular components:

$$\mathbf{J}_{n\to+} = -q\int_{U_{c-}}^{\infty}\int_{0}^{\infty}\mathbf{v}_x g(E) f(E) dE_{yz} dE_x - q\int_{0}^{U_{c-}}\int_{0}^{\infty}\mathbf{v}_x T_n(E) g(E) f(E) dE_{yz} dE_x \tag{40}$$

The integration of (40) over the parallel energy, E_{yz}, using Fermi-Dirac statistics yields

(see Derivation 2 in Appendix G):

$$\mathbf{J}_{n\to+} = -A_n^* \frac{T_{n-}}{k}\left(\underbrace{\int_{U_{c-}}^{\infty} \ln\left(1+e^{h_c - E_x/kT_n}\right)dE_x}_{\text{Thermionic Emission}} + \underbrace{\int_{0}^{U_{c-}} T_n\left(E_x\right)\ln\left(1+e^{h_c - E_x/kT_n}\right)dE_x}_{\text{Tunneling}} \right) \quad (41)$$

where A_n^* is the Richardson constant given by:

$$A_n^* = \frac{q m_n^* k^2}{2p^2\hbar^3} \quad (42)$$

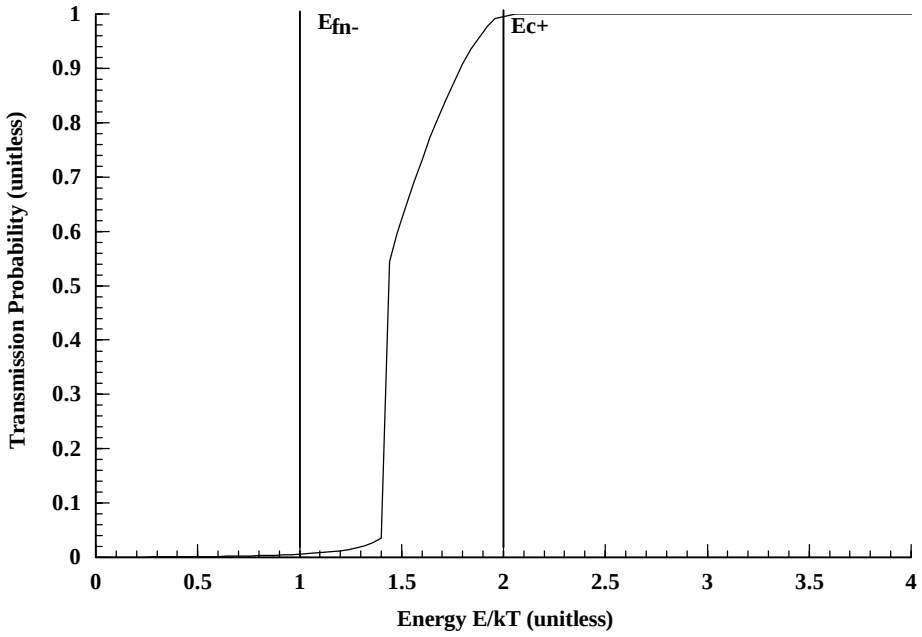

Figure 5 - Transmission probability versus energy for the barrier in Figure 4

Equation (41) only represents the carriers moving from left to right. A similar expression applies to carriers moving from right to left. Under equilibrium conditions, these two currents must be equal. Equation (41) supports this because the following two conditions are true. First, the Richardson constant uses the lighter mass of the two materials. This accounts for the possible total internal reflection of carriers when

moving from a heavier mass material to a lighter mass material [20,21]. In this case, the transmission probability is the probability that a carrier, which does not undergo total internal reflection, will cross over or though the barrier. Second, the transmission probability for carriers moving from left to right is the same for carriers moving from right to left. With these two conditions the total current will be zero when the quasi-fermi levels are constant across the band discontinuity.

Figure 6 shows plots the integrand of (41) for the barrier shown in Figure 4 using both Boltzmann and Fermi-Dirac statistics. The area under these curves is the current for carriers moving from left to right. As expected, Boltzmann statistics approximates Fermi-Dirac at higher energies. Usually discussions of thermionic emission current employ Boltzmann statistics in which case the first integral in (41) reduces to a simple exponential. This integral does have an analytical solution even for Fermi-Dirac statistics. The second integral in (41) does not in general have an analytical solution due to the direct dependence of the transmission probability on the band edge. SimWindows uses the analytical expression below for the thermionic emission current, and uses a numerical integral for the tunneling current.

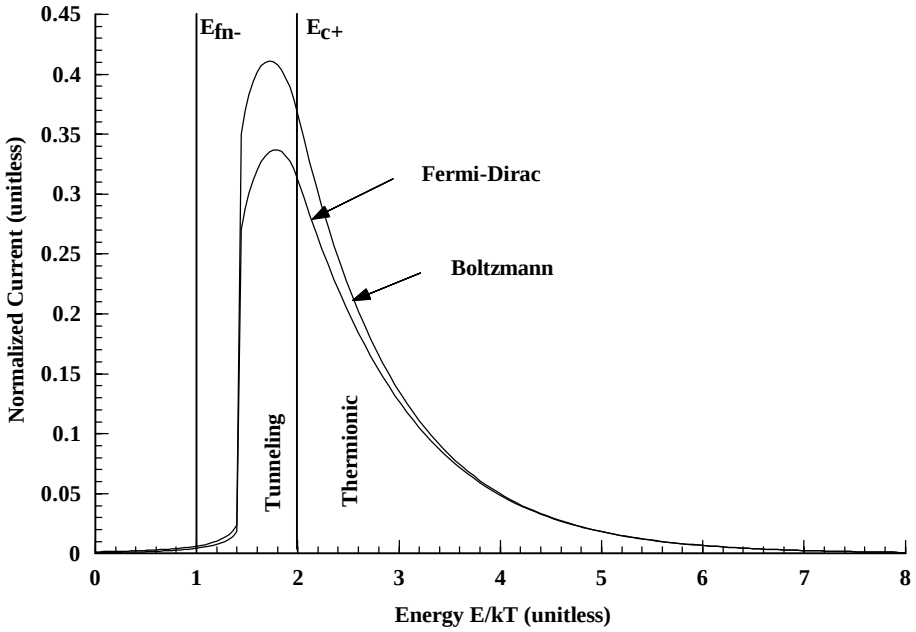

Figure 6 - Current versus energy for the barrier in Figure 4

It is quite simple to evaluate the thermionic emission integral in (41) assuming a Boltzmann distribution function, and the resulting expression is:

$$\mathbf{J}_{n-\to+}^{therm} = -A_n^* T_{n-}^2 e^{h_{c-}-U_{c-}/kT_{n-}} \tag{43}$$

For device simulations it is impossible to predict that the Boltzmann approximation will be valid under all circumstances. An equivalent expression for the current that uses the Fermi-Dirac distribution function would ensure that SimWindows uses a valid expression under all conditions. The analytical solution for the thermionic emission current using Fermi-Dirac statistics is (see Derivation 2 in Appendix G):

$$\mathbf{J}_{n-\to+}^{therm} = -A_n^* T_{n-}^2 \left\{ \mathrm{Li}_2\left(\frac{1}{1+e^{-(h_{c-}-U_{c-}/kT_{n-})}} \right) + \frac{1}{2}\left[\ln\left(1+e^{(h_{c-}-U_{c-}/kT_{n-})}\right) \right]^2 \right\} \tag{44}$$

where $Li_2(x)$ is the dilogarithm function (see Appendix H). Equation (44) is a difficult equation to interpret intuitively as compared with equation (43). Equation (43) approximates (44) when the quasi-fermi level is far away from the top of the barrier.

Figure 7 illustrates this by plotting the normalized current versus barrier height for an electron quasi-fermi level 1 kT above the conduction band. Since (43) and (44) are just functions of the difference between the quasi-fermi level and the top of the barrier, the energy level of the bottom of the barrier is not important in controlling the current.

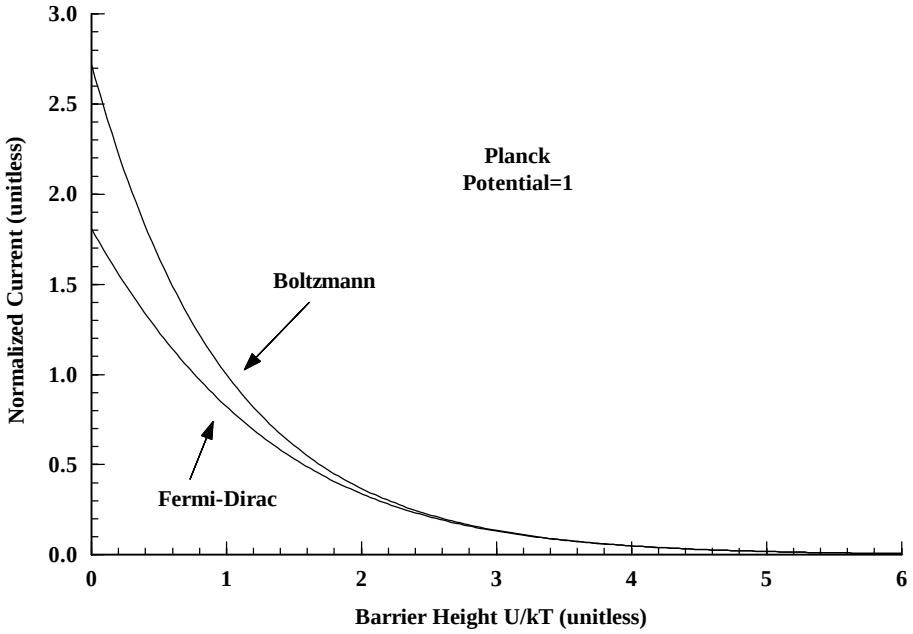

Figure 7 - Normalized thermionic emission current versus barrier height

2.2.3.3 Recombination/Generation

SimWindows presently incorporates four recombination and generation mechanisms. They are spontaneous band-to-band (b-b) recombination, Shockley-Hall-Reed (SHR) recombination, external optical generation, and stimulated emission. Section 2.3 discusses external optical generation and stimulated emission. The spontaneous and SHR recombination expressions for bulk materials are:

$$U_{b-b} = B(np - n_i^2) \tag{45}$$

$$U_{shr} = \frac{np - n_i^2}{(p + n_i)t_{no} + (n + n_i)t_{po}} \tag{46}$$

where the SHR recombination expression (46) always assumes that the trap level is located at the intrinsic level of the material.

For quantum well regions, the recombination expressions differ to take into account the two dimensional nature of the carriers and their corresponding wavefunctions.

$$U_{b-b} = \frac{1}{L_{qw}} \left| \int_0^{L_{qw}} \psi_n(x) \psi_p(x) dx \right|^2 B_{qw} (n_{2d} p_{2d} - n_{i,2d}^2) \tag{47}$$

$$U_{shr} = \frac{1}{L_{qw}} \left| \int_0^{L_{qw}} \psi_n(x) \psi_p(x) dx \right|^2 \frac{n_{2d} p_{2d} - n_{i,2d}^2}{(p_{2d} + n_{i,2d})t_{no} + (n_{2d} + n_{i,2d})t_{po}} \tag{48}$$

These expressions modify the bulk recombination expressions by replacing the three-dimensional carrier concentration in equations (45) and (46) by the two-dimensional carrier concentrations in the quantum well. An overlap integral multiplies this result to take into account the matching between electron and hole wavefunctions [22]. These expressions (in units of cm^{-2} s^{-1}) then distribute the recombination rate equally over the quantum well by dividing by the length of the quantum well. The net result is a recombination rate (in units of cm^{-3} s^{-1}) that is compatible with the current continuity equations given in (25) and (26).

2.2.4 Boundary Conditions

To complete the electrical model, there are certain boundary conditions for the three fundamental variables. SimWindows presently uses only ohmic boundary conditions where it assumes that there is no voltage drop across the contact and there

is an infinite surface recombination rate at the contact. This implies that under all device operating conditions, the potential on the left contact is equal to the applied bias on the left contact. The potential on the right contact is equal to the applied bias on the right contact plus the built in potential. Since there is an infinite recombination rate at the contact, the electron and hole Planck potentials retain their equilibrium values. Relations (49) through (51) represent these boundary conditions.

$$f(0) = V_l \qquad f(L) = f_0 + V_r \tag{49}$$

$$h_c(0) = h_{c0}(0) \qquad h_c(L) = h_{c0}(L) \tag{50}$$

$$h_v(0) = h_{v0}(0) \qquad h_v(L) = h_{v0}(L) \tag{51}$$

These boundary conditions are sufficient for the devices presented here, but there are other boundary conditions that are useful for different devices. These include Schottky contacts and finite surface recombination boundary conditions. Future work could include incorporating these boundary conditions into SimWindows.

2.3 Photons

SimWindows uses a photon model that allows it to simulate solar cells and certain types of semiconductor lasers. SimWindows recognizes that photons generated externally differ from photons generated internally. This optical model stems largely from the need to simulate vertical cavity surface emitting lasers that use Bragg reflectors instead of metallic mirrors. These structures are quite different from edge emitting lasers and the corresponding equations are more complex. Therefore, SimWindows simulates only surface emitting lasers. Future work includes extending SimWindows to handle edge emitting lasers.

This section consists of three parts that outline the complete photon model. Section 2.3.1 describes how SimWindows handles the electromagnetic reflections of material interfaces. Interface reflections is an important feature of SimWindows. Section 2.3.2 shows its use in solar cell applications, and section 2.3.3 shows its use in semiconductor lasers structures.

2.3.1 Interface Reflections

Interface reflections play an important role in this optical model. Since many semiconductor devices incorporate a variety of different materials, the reflection of photons through the device is a useful feature. VCSEL simulations require this feature, but it can also improve the simulation of solar cells.

SimWindows uses a transmission matrix method [23] to calculate electromagnetic fields within device structures. The idea is to use a simple 2x2 matrix to describe the propagation of an electromagnetic field from one section to another section of the device. For each discrete section there is a unique 2x2 matrix. Multiplying the matrices will describe how the wave propagates through the entire device. Figure 8 shows the arrangement of forward and reverse propagating fields.

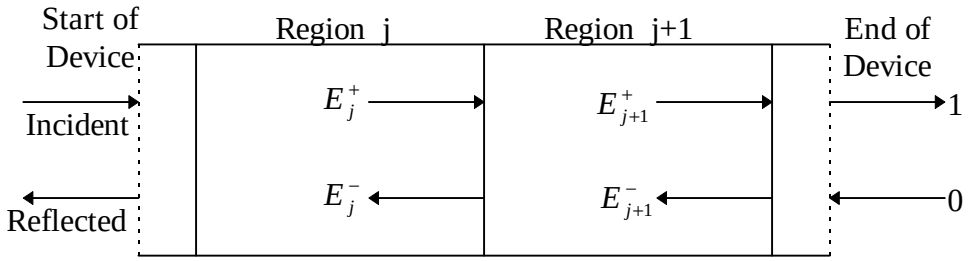

Figure 8 - Arrangement of forward and reverse propagating fields

Equation (52) gives the total field within the jth region where the first term is the forward propagating component and the second term is the reverse propagating component.

$$E_j = E_j^+ e^{i\left(wt - k_o n_j \left(x - x_j\right)\right)} + E_j^- e^{i\left(wt + k_o n_j \left(x - x_j\right)\right)} \tag{52}$$

In this equation k_o is the free space wave vector, and n_j is the complex refractive index. The corresponding magnetic field is:

$$H_j = \frac{E_j^+}{Z_j} e^{i\left(wt - k_o n_j \left(x - x_j\right)\right)} - \frac{E_j^-}{Z_j} e^{i\left(wt + k_o n_j \left(x - x_j\right)\right)} \tag{53}$$

where Z_j is the complex impedance of the region. The complex refractive index and the complex impedance are related to the real refractive index, the absorption coefficient, the free space wavevector, k_0, and the free space impedance, Z_0, through the relations:

$$n_j = n_{real} - i\frac{a}{2k_0} \qquad Z_j = \frac{Z_0}{n_j} \tag{54}$$

The matrix method determines the magnitudes of the forward and reverse propagating fields in the jth+1 region based on the magnitudes in the jth region. Equation (55) represents this procedure:

$$\begin{bmatrix} E_{j+1}^+ \\ E_{j+1}^- \end{bmatrix} = \left\{ \begin{bmatrix} e^{-ik_0 n_{j+1}\left(x_{j+1} - x_j\right)} & 0 \\ 0 & e^{ik_0 n_{j+1}\left(x_{j+1} - x_j\right)} \end{bmatrix} \right\} \left\{ \frac{1}{2Z_j} \begin{bmatrix} Z_j + Z_{j+1} & Z_j - Z_{j+1} \\ Z_j - Z_{j+1} & Z_j + Z_{j+1} \end{bmatrix} \right\} \begin{bmatrix} E_j^+ \\ E_j^- \end{bmatrix} \tag{55}$$

where the second matrix propagates the fields across the boundary between regions where the impedance changes, and the first matrix propagates the fields through the region where the impedance is constant. Multiplying the two matrices yields:

$$\begin{bmatrix} E_{j+1}^{+} \\ E_{j+1}^{-} \end{bmatrix} = \frac{1}{2Z_j} \begin{bmatrix} \left(Z_j + Z_{j+1}\right) e^{-ik_0 n_{j+1}\left(x_{j+1}-x_j\right)} & \left(Z_j - Z_{j+1}\right) e^{-ik_0 n_{j+1}\left(x_{j+1}-x_j\right)} \\ \left(Z_j - Z_{j+1}\right) e^{ik_0 n_{j+1}\left(x_{j+1}-x_j\right)} & \left(Z_j + Z_{j+1}\right) e^{ik_0 n_{j+1}\left(x_{j+1}-x_j\right)} \end{bmatrix} \begin{bmatrix} E_j^{+} \\ E_j^{-} \end{bmatrix} \tag{56}$$

Inverting this equation yields an equation that propagates fields in the opposite direction:

$$\begin{bmatrix} E_j^{+} \\ E_j^{-} \end{bmatrix} = \frac{1}{2Z_{j+1}} \begin{bmatrix} \left(Z_{j+1} + Z_j\right) e^{ik_0 n_{j+1}\left(x_{j+1}-x_j\right)} & \left(Z_{j+1} - Z_j\right) e^{-ik_0 n_{j+1}\left(x_{j+1}-x_j\right)} \\ \left(Z_{j+1} - Z_j\right) e^{ik_0 n_{j+1}\left(x_{j+1}-x_j\right)} & \left(Z_{j+1} + Z_j\right) e^{-ik_0 n_{j+1}\left(x_{j+1}-x_j\right)} \end{bmatrix} \begin{bmatrix} E_{j+1}^{+} \\ E_{j+1}^{-} \end{bmatrix} \tag{57}$$

To use (56) or (57) to calculate the electromagnetic field within the device, the magnitudes of the field at one end of the device are set to one and zero as shown in Figure 8. In the case shown, light is incident from the left. Therefore, the reverse propagating field at the right side of the device must be zero, and the forward propagating field is arbitrarily set to one. Recursively applying equation (57) yields the magnitude of the field in all regions of the device. SimWindows also takes into account the refractive index in the external regions to the left and right of the device. The user can specify the refractive index in the external regions but SimWindows assumes that these regions are lossless.

2.3.2 External Optical Generation

When performing simulations on photodetectors or solar cells, SimWindows must use the calculated electromagnetic fields as well as the specified input optical power to compute the carrier generation rate. The current continuity equations then combine the generation rate with the other recombination processes. Since optical power is the measurable quantity, the first step in the calculation of the optical generation rate is to compute the time averaged Poynting vector for the fields given in (52) and (53). The average Poynting vector in each region is:

$$\left\langle \mathbf{S}_j \right\rangle = \tfrac{1}{2}\left[\mathbf{E}_j \times \mathbf{H}_j^*\right] \tag{58}$$

Using the fields in equations (52) and (53), the average Poynting vector is:

$$\left\langle S_j \right\rangle = \left\langle S_j^+ \right\rangle - \left\langle S_j^- \right\rangle + \Re\left[\frac{i\Im\left(E_j^- E_j^{+*} e^{i\left(2k_0\Re\left(n_j\right)\left(x-x_j\right)\right)}\right)}{Z_j^*}\right] \tag{59}$$

where the Poynting vectors of the individual waves are:

$$\left\langle S_j^+ \right\rangle = \tfrac{1}{2}\left|E_j^+\right|^2 e^{-a\left(x-x_j\right)}\Re\left(\tfrac{1}{Z_j^*}\right) \qquad \left\langle S_j^- \right\rangle = \tfrac{1}{2}\left|E_j^-\right|^2 e^{a\left(x-x_j\right)}\Re\left(\tfrac{1}{Z_j^*}\right) \tag{60}$$

In (59) and (60), $\Re$ and $\Im$ are real and imaginary components, respectively. The total Poynting vector in units of W cm^{-2} is a measure of the total amount of optical energy crossing a plane per unit time. Equation (59) is zero in the case of a lossless medium with a perfect reflector which reflects all of the incident power. In the case of no reflection, either the forward or reverse propagating fields is zero depending on the direction of the incoming light. Under these circumstances, the third term in (59) is zero and the total Poynting vector is just the Poynting vector of the single propagating wave.

Until this point the values of the field and the Poynting vectors are arbitrary since the starting point for applying (56) and (57) is to set the magnitude of the fields to one and zero. Since the user specifies the incident optical power, the next step is to rescale the values of the Poynting vectors to correspond to the given incident power. Since (56) and (57) are linear equations, multiplying the Poynting vectors in all the regions by the same factor will rescale the incident Poynting vector to the given incident optical power. The Poynting vectors are now in units of W cm^{-2}. Equation

(60) will rescale the magnitudes of the fields to correspond to the incident Poynting vectors. Equation (59) will now correctly calculate the total Poynting vector.

The final step is to calculate the optical power absorbed by the semiconductor to generate carriers. Differentiating (59) with respect to *x* will give the change in the power carried by the electromagnetic wave.

$$\left.\frac{d\langle S_j\rangle}{dx}\right|_{x=x_j} = -a\langle S_j^+\rangle - a\langle S_j^-\rangle + k_0\Re(n_j)\Re\left[\frac{2i\Re\left(E_j^- E_j^{+*}\right)}{Z^*}\right] \tag{61}$$

Since (61) is the change in the power of the electromagnetic wave, the negative is the power supplied to the semiconductor. Dividing by the photon energy will yield the number of carriers generated per volume per time. SimWindows can also accept a spectrum of incident photons. It will repeat this procedure for each photon energy in the spectrum. The total result for the optical generation rate is just the sum of the optical generation rate for each photon energy:

$$G_{opt}(x) = \sum_{hu_{opt}} G_{u,opt}(x) = \sum_{hu_{opt}} \left(\frac{a\langle S_j^+\rangle + a\langle S_j^-\rangle - k_0\Re(n_j)\Re\left[\frac{2i\Re\left(E_j^- E_j^{+*}\right)}{Z^*}\right]}{hu_{opt}} \right) \tag{62}$$

The following figures demonstrates the interface reflections and optical generation features of SimWindows using the device file in Listing 1 of Appendix B. Figure 9 shows the equilibrium band diagram of an $Al_{0.4}Ga_{0.6}As$ solar cell with 10 GaAs quantum wells in the intrinsic region. Figure 10 shows the optical generation rate for an AM1.5 input spectrum [24] with interface reflections on and off. Since interface reflections also take into account reflections at the ends of the device, Figure 10 shows an overall decrease in the optical generation rate due to a reflection at the

front interface as well as a periodic generation rate through the device due to the multiple interfaces from the quantum wells.

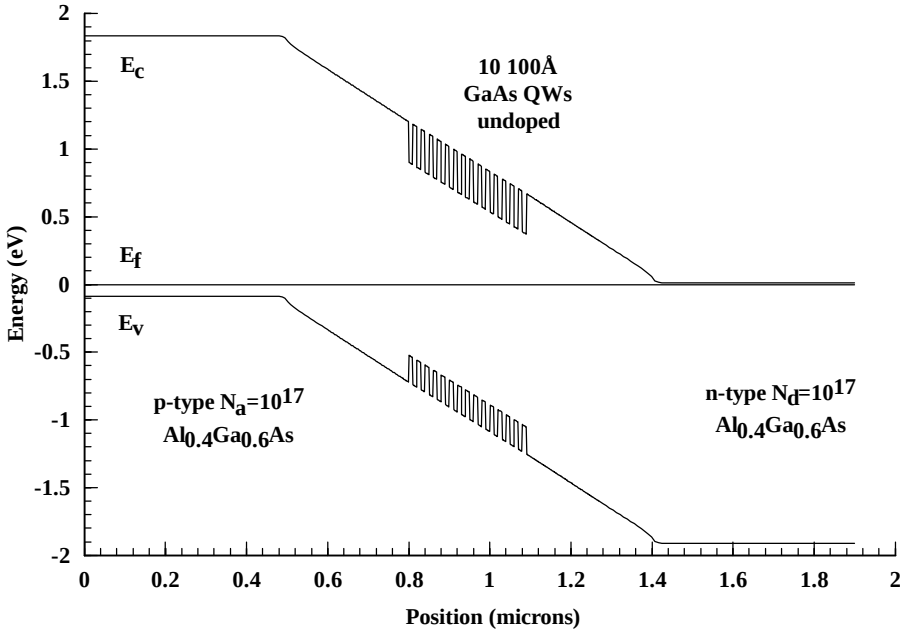

Figure 9 - Equilibrium band diagram for a 10 QW solar cell

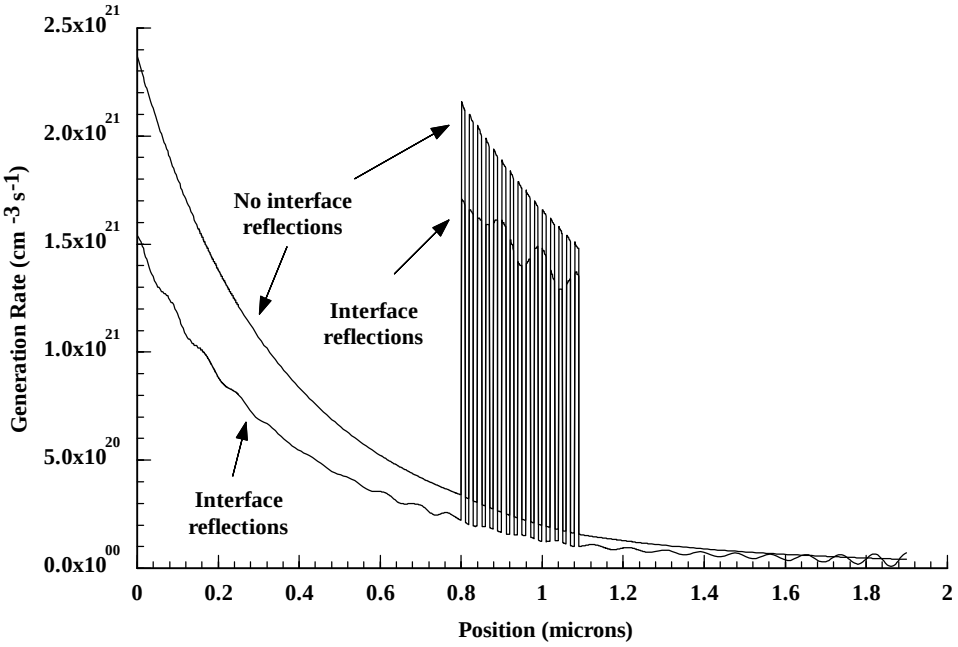

Figure 10 - Optical generation rate for the structure in Figure 9 using AM1.5

2.3.3 Stimulated Emission

The second application that utilizes interface reflections is stimulated emission. Stimulated emission is more complicated than external optical generation because it requires three components: the electromagnetic field profile - $\mathcal{E}(x)$, the local gain - $g(x)$, and the total number of photons in the lasing mode - S. The total number of photons in the lasing mode is a new fundamental variable that SimWindows solves iteratively. It differs from the other fundamental variables in that it is position independent, and requires solving a new position independent equation that depends on the results of the electrical calculations. SimWindows presently simulates only one lasing mode which is sufficient for VCSELs which typically have only one longitudinal mode. Future work could include incorporating multiple mode calculations into SimWindows.

The interface reflection calculation can determine both the lasing wavelength of the DBR laser and the electromagnetic field profile at that lasing wavelength. SimWindows determines the lasing wavelength by searching for a local minimum in the reflectivity versus wavelength for the laser structure. SimWindows calculates the reflectivity by using the same arrangement of fields as in Figure 8. SimWindows varies the wavelength of photons incident on the device and computes the reflectivity from the reflected and incident intensities. SimWindows performs this calculation at all operating conditions of the device, not just at equilibrium. If material properties change during the simulation (for instance due to temperature changes), then SimWindows can track the shift in the lasing wavelength. Figure 11 shows a reflectivity versus wavelength plot for a DBR laser and labels the lasing wavelength. Since there are many local minima, SimWindows requires a starting wavelength close to the actual wavelength for the search to be successful.

Figure 12 shows the square of the magnitude of the computed field profile at a wavelength corresponding the wavelength labeled in Figure 11. SimWindows used the VCSEL device file in Listing 2 in Appendix B to generate these plots. To use the field shape to calculate stimulated emission, the square of the magnitude is normalized to one:

$$A_c \int_0^L \left| \mathcal{E}_{stim}(x) \right|^2 dx = 1 \tag{63}$$

where A_c is the area of the cavity. This gives $\mathcal{E}_{stim}(x)$ the units of $cm^{-3/2}$. The physical reason for performing this normalization appears below.

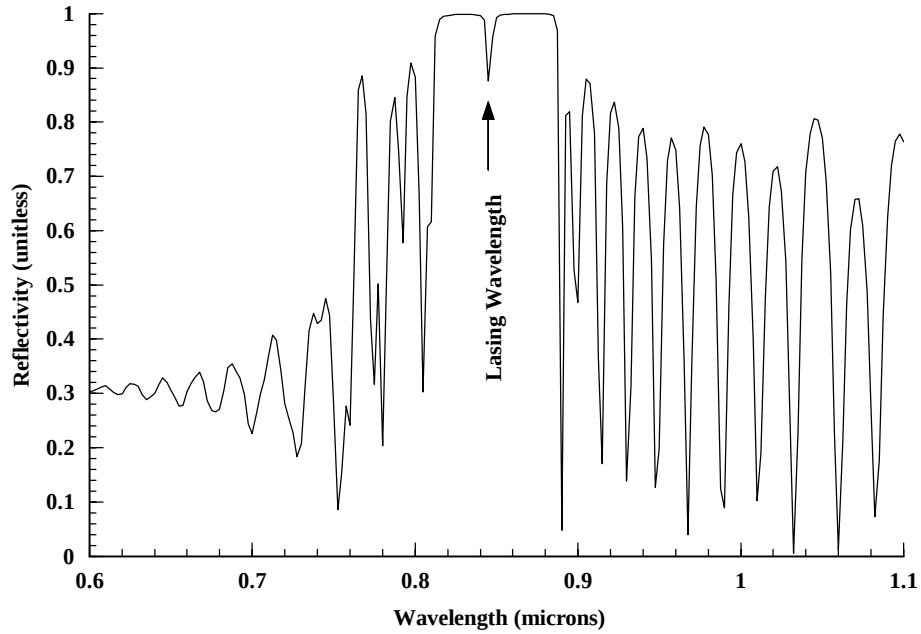

Figure 11 - Reflectivity versus wavelength for a typical DBR laser

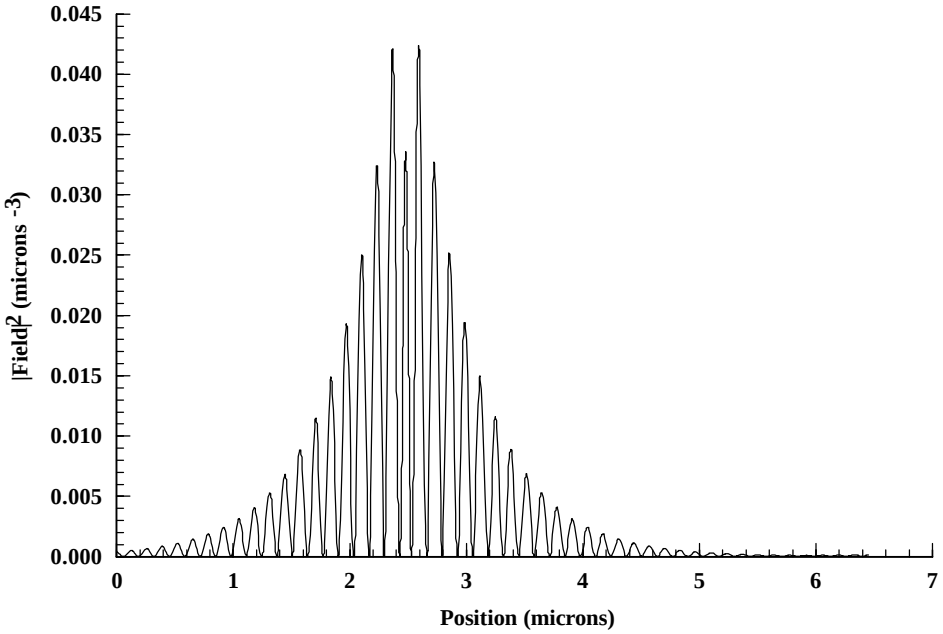

Figure 12 - Square of the field magnitude for a DBR laser

The second component for calculating the stimulated recombination rate is the local gain. Since many texts on semiconductor lasers [25,26] outline the derivation of gain and stimulated emission, this thesis will not present it in great detail. The definition of local gain is the optical power emitted per unit volume divided by the optical power crossing the volume:

$$g(u_{stim}) = \frac{1}{I(u_{stim})}\frac{dI(u_{stim})}{dx} = \frac{\text{Power emitted / volume}}{\frac{\text{Power}}{\text{Area}}\ \text{crossing volume}} \tag{64}$$

If the optical intensity increases as photons pass through the region, then the derivative in (64) is positive and there is gain. If the optical intensity decreases then there is absorption.

Since stimulated emission involves a photon inducing an electron and hole to recombine and emit another photon, only certain electrons and holes at given energies will recombine. The energy of the electrons and holes contributing to stimulated emission is:

$$E_{n,stim} = \frac{m_p^*}{m_n^* + m_p^*}\left(hu_{stim} - E_g\right) + E_c \tag{65}$$

$$E_{p,stim} = E_v - \frac{m_n^*}{m_n^* + m_p^*}\left(hu_{stim} - E_g\right) \tag{66}$$

where u_{stim} is the frequency of the lasing photons. These assume that the momentum of the photon is negligible and the momentum of the electron is equal to the momentum of the hole. This assumption does introduce a small error in the values of $E_{n,stim}$ and $E_{p,stim}$. Figure 13 shows these energy levels on an E versus k diagram.

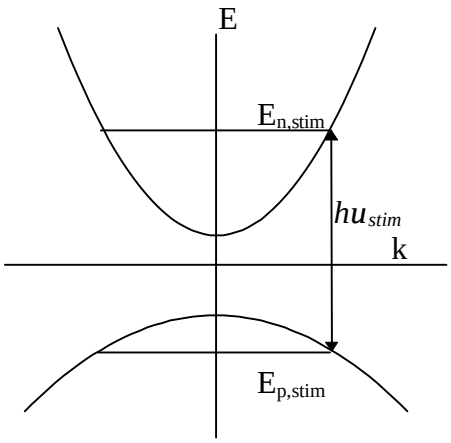

Figure 13 - Energy levels for stimulated emission

Similar equations for quantum wells take into account the electron and hole quantized energy levels, E_{qwn} and E_{qwp} [26]:

$$E_{n,stim} = \frac{m_p^*}{m_n^* + m_p^*}\left(hu_{stim} - E_{gqw}\right) + E_{qwn} + E_c \tag{67}$$

$$E_{p,stim} = E_v - \frac{m_n^*}{m_n^* + m_p^*}\left(hu_{stim} - E_{gqw}\right) - E_{qwp} \tag{68}$$

Fermi's Golden Rule in conjunction with (65) through (68) will yield the transition rate for an electron in the conduction band to recombine with a hole in the valence band and emit a photon. This leads to the local gain expression in (69) below, where the gain depends on the absorption coefficient, the probability that an electron is at energy $E_{n,stim}$, and the probability that an electron is at energy $E_{p,stim}$. For there to be gain, there must be a population inversion where there is a greater probability that electrons will occupy an energy $E_{n,stim}$ than occupy an energy $E_{p,stim}$. Equation (69) uses the absorption coefficient instead of several prefactors that appear in the usual derivation of the local gain [27]. Since the absorption coefficient is a material parameter, this allows the user more direct control over the gain in the laser.

$$g(hu_{stim}) = a(hu_{stim})\left[f\left(E_{n,stim}\right) - f\left(E_{p,stim}\right)\right] \tag{69}$$

SimWindows assumes with this equation that the maximum gain in the active region is equal to the maximum absorption. This is not strictly true since there are absorption processes such as exciton absorption which do not contribute to the maximum gain of the laser.

With the electric field and the local gain, SimWindows calculates the position dependent stimulated recombination rate using [5,7]:

$$U_{stim}(x) = v_{stim} g(x) \underbrace{S\left|\mathcal{E}_{stim}(x)\right|^2}_{\substack{\text{Photon} \\ \text{Density cm}^{-3}}} \tag{70}$$

where v_{stim} is the group velocity of the photons. The physical significance of normalizing the electric field is now clear. Normalizing the electric field allows the total number of photons in the mode, *S*, times the square of the field profile to correspond to the position dependent photon density at each point in device. This is exactly analogous to distributing the total number of carriers in a quantum well over the length of the quantum well using the carrier wavefunction.

The third component for the stimulated emission is the total number of photons in the lasing mode, *S*. A steady state solution of equation (71) in conjunction with the electronic equations will yield the total number of photons:

$$\tilde{U}_{stim} + b\tilde{U}_{b-b} - S/t_{ph} = \frac{dS}{dt} \tag{71}$$

where the first two terms represent the total gain in the number of photons per unit time due to stimulated and spontaneous emission. These terms are the integral of the

total stimulated and spontaneous recombination rates over the total volume of the cavity. The user specifies the spontaneous emission factor b which represents the fraction of spontaneously generated photons that actually excite the lasing mode. Measurements on vertical cavity lasers [28] as well as traditional expressions for double heterostructure lasers [29] can yield the spontaneous emission factor. The last term in (71) is the loss of photons per unit time. The photon lifetime, t_{ph}, includes the distributed mirror loss, a_m, as well as the user specified scattering loss, a_s:

$$t_{ph} = \frac{1}{v_{stim}\left(a_m + a_s\right)} \tag{72}$$

where:

$$a_m = \frac{1}{2L_c}\ln\left(\frac{1}{R_l R_r}\right) \tag{73}$$

In this equation R_l and R_r are the effective mirror reflectivities and L_c is the effective cavity length. The user must specify all of these quantities. Since VCSEL structures use distributed Bragg reflectors, these parameters are effective quantities that model the structure as two mirrors separated by an effective cavity length [30].

Despite its simplicity, equation (71) is not easy to solve for the total number of photons. The primary difficulty is that the stimulated emission not only directly depends on S, but it also indirectly depends on S through the local gain. Since the expression for the local gain uses the electron and hole quasi-fermi levels, the stimulated emission depends on the result of the electronic equations. However, the value of the stimulated emission influences the electronic equations. This means that the solution to equation (71) must be self-consistent with the electronic equations.

This feedback mechanism between the electrical and optical equations is representative of the actual physical feedback mechanism that takes place in semiconductor lasers. When the bias across a semiconductor laser increases, the quasi-fermi level separation will increase causing the gain to increase. This results in a higher stimulated emission rate which acts to reduce the separation of the quasi-fermi levels, and reduce the gain. This feedback will achieve a steady state balance between the quasi-fermi levels, the gain, and the stimulated emission rate. This is why gain saturation occurs in semiconductor lasers.

2.4 Energy

The electrical and optical models in the previous sections are sufficient when thermal properties of a device are unimportant. Many devices currently under research, including VCSELs, display certain properties that only thermal effects can explain. Therefore, SimWindows incorporates the equations that govern the device temperature.

A discussion of device temperature actually includes four systems of interest: the electrons, the holes, the lattice, and the environment. A key assumption is that new particles added to any of the systems instantly thermalize with the population. Their energy redistributes over the whole population such that an equilibrium distribution always describes the energy of the particles in each system. As a result, the temperature of the system is a measure of the average energy of all particles in the system. Since the separate systems exchange energy, the temperatures adjust so that in steady state, each system gains energy at the same rate that it loses energy. The environment is a special system that acts as an infinite reservoir of energy. The

temperature of the environment is a known value and used as a boundary condition, but it is useful to discuss the environment here and how it relates to the other systems.

The next three sections discuss various thermal models that a semiconductor device simulator can incorporate. Section 2.4.1 discusses the complete “Three Temperature Model” where the temperature of the electrons, holes, and lattice are all different. SimWindows does not presently implement this model, but SimWindows does implement two simpler models which result from assumptions on the Three Temperature Model. Section 2.4.2 describes the “Single Temperature Model” where SimWindows assumes that one temperature describes the electrons, holes, and lattice. Section 2.4.3 describes the “Hot Electron Model” where SimWindows assumes that only the electron temperature deviates from the environment temperature.

2.4.1 Three Temperature Model

The three temperature model is the most general model where a separate temperature describes the electrons, holes, and lattice. The equations that govern the three temperatures are very similar to the electrical equations except that the equations govern energy instead of charge. This section first presents the rate equations for the electron, hole, and lattice energy. These rate equations represent a balance between energy flux and the energy loss in the device. This section then presents the equations for energy flux followed by the relations for the energy loss.

2.4.1.1 Rate Equations

The solution for the three fundamental temperatures require three rate equations, (74) to (76), for the electron hole and lattice energies. SimWindows presently uses these equations only in steady state.

$$\nabla \bullet \mathbf{S}_n^{tot}(x) + W_n^{tot}(x) = \frac{\partial u_n}{\partial t} \tag{74}$$

$$\nabla \bullet \mathbf{S}_p^{tot}(x) + W_p^{tot}(x) = \frac{\partial u_p}{\partial t} \tag{75}$$

$$\nabla \bullet \mathbf{S}_{lat}(x) - W_{lat}(x) = \frac{\partial u_{lat}}{\partial t} \tag{76}$$

In these equations, **S** is the total energy flux (J cm^{-2} s^{-1}) and *W* is the total energy loss per volume (J cm^{-3} s^{-1}). Since the terms in these equations represent the total energy instead of just the kinetic energy, which the literature often presents [17,31], equations (74) and (75) do not explicitly include the joule heating terms $\mathbf{J}_{n,p} \bullet \nabla E_{c,v}$. With the definitions of **S** and *W* below, these equations are mathematically equivalent to the equations for kinetic energy and implicitly include the joule heating terms. This section will elaborate on this point further after the discussion of **S** and *W*.

2.4.1.2 Energy Flux

Solving equations (74) through (76) require expressions for the energy flux, **S**. The derivation of the carrier energy flux is similar to the current. The starting expression for the derivation is the integral:

$$\mathbf{S}^{tot} = \frac{1}{4\pi^3} \iiint \mathbf{v} E f dk_x dk_y dk_z \tag{77}$$

This expression is exactly analogous to equation (27) for the current except that the total energy of the carrier replaces the charge of the carrier. Since the total energy is the sum of the kinetic and potential energies, equation (77) can be split into two terms. For electrons, the total energy flux is:

$$\mathbf{S}_n^{tot} = \frac{1}{4p^3}\iiint \mathbf{v}(E - E_c)\, f dk_x dk_y dk_z + \frac{E_c}{4p^3}\iiint \mathbf{v} f dk_x dk_y dk_z \tag{78}$$

The first integral is the flux of kinetic energy where E-E_c is the kinetic energy of each electron. The second integral is the flux of potential energy where the band edge, E_c, is the potential energy of each electron. The second integral is related to the current and equation (78) yields:

$$\mathbf{S}_n^{tot} = \frac{1}{4p^3}\iiint \mathbf{v}(E - E_c)\, f dk_x dk_y dk_z + \frac{E_c \mathbf{J}_n}{-q} \tag{79}$$

Using the same methods in the derivation of the current expressions, the solution to equation (79) yields the energy flux equations for drift diffusion, thermionic emission, and tunneling.

2.4.1.2.1 Drift-Diffusion

Using the same approximations to the Boltzmann transport equations from section 2.2.3.2.1 for the drift diffusion current, the expressions for the electron and hole drift diffusion energy flux are:

$$\mathbf{S}_n^{tot} = -m_n n \frac{kT_n}{q}\left\{\begin{array}{l}\left(kT_n \nabla h_c + \nabla E_c\right)\left(\frac{5}{2} + u_n\right)\frac{F_{3/2+u_n}(h_c)}{F_{1/2+u_n}(h_c)} \\ +\nabla kT_n\left(\frac{7}{2} + u_n\right)\left(\frac{5}{2} + u_n\right)\frac{F_{5/2+u_n}(h_c)}{F_{1/2+u_n}(h_c)}\end{array}\right\} + \frac{E_c \mathbf{J}_n}{-q} \tag{80}$$

$$\mathbf{S}_p^{tot} = -m_p p \frac{kT_p}{q}\left\{\begin{array}{l}\left(kT_p \nabla h_v - \nabla E_v\right)\left(\frac{5}{2} + u_p\right)\frac{F_{3/2+u_p}(h_v)}{F_{1/2+u_p}(h_v)} \\ +\nabla kT_p\left(\frac{7}{2} + u_p\right)\left(\frac{5}{2} + u_p\right)\frac{F_{5/2+u_p}(h_v)}{F_{1/2+u_p}(h_v)}\end{array}\right\} - \frac{E_v \mathbf{J}_p}{q} \tag{81}$$

These equations are analogous to equations (32) and (33) for the current. Again applying equation (34) for the gradient of the Planck potential, equations (80) and (81) yield the standard generalized drift diffusion equations [17]:

$$\mathbf{S}_n^{tot} = -\left(\tfrac{5}{2}+u_n\right)\tfrac{F_{3/2+u_n}(h_c)}{F_{1/2+u_n}(h_c)}m_n\frac{kT_n}{q}\begin{Bmatrix} kT_n\,\tfrac{F_{1/2}(h_c)}{F_{-1/2}(h_c)}\nabla n + n\nabla E_c \\ -\tfrac{3}{2}kT_n n\,\tfrac{F_{1/2}(h_c)}{F_{-1/2}(h_c)}\nabla\ln(m_n^*) \\ +n\left(\left(\tfrac{7}{2}+u_n\right)\tfrac{F_{5/2+u_n}(h_c)}{F_{3/2+u_n}(h_c)} - \tfrac{3}{2}\tfrac{F_{1/2}(h_c)}{F_{-1/2}(h_c)}\right)\nabla kT_n \end{Bmatrix} + \tfrac{E_c\mathbf{J}_n}{-q} \quad (82)$$

$$\mathbf{S}_p^{tot} = -\left(\tfrac{5}{2}+u_p\right)\tfrac{F_{3/2+u}(h_v)}{F_{1/2+u}(h_v)}m_p\frac{kT_p}{q}\begin{Bmatrix} kT_p\,\tfrac{F_{1/2}(h_v)}{F_{-1/2}(h_v)}\nabla p - p\nabla E_v \\ -\tfrac{3}{2}kT_p p\,\tfrac{F_{1/2}(h_v)}{F_{-1/2}(h_v)}\nabla\ln(m_p^*) \\ +p\left(\left(\tfrac{7}{2}+u_p\right)\tfrac{F_{5/2+u_p}(h_v)}{F_{3/2+u_p}(h_v)} - \tfrac{3}{2}\tfrac{F_{1/2}(h_v)}{F_{-1/2}(h_v)}\right)\nabla kT_p \end{Bmatrix} - \tfrac{E_v\mathbf{J}_p}{q} \quad (83)$$

2.4.1.2.2 Thermionic Emission and Tunneling

The derivation for the thermionic emission and tunneling energy flows proceeds in the same manner as the derivation for the thermionic emission and tunneling current. The total energy flux associated with thermionic emission and tunneling current is:

$$\mathbf{S}_{n-\to+}^{tot} = \underbrace{\int_{U_{c-}}^{\infty}\mathbf{v}_x(E-E_c)g(E)f(E)dE}_{\text{Thermionic Emission}} + \underbrace{\int_{0}^{U_{c-}}\mathbf{v}_x T_n(E)(E-E_c)g(E)f(E)dE}_{\text{Tunneling}} + \frac{E_{c-}\mathbf{J}_{n-\to+}}{-q} \quad (84)$$

After splitting the energy terms into parallel and perpendicular components and integrating over the parallel energy terms, the first integral in equation (84) yields the following for Boltzmann statistics (see Derivation 3 in Appendix G):

$$\mathbf{S}_{n-\to+}^{therm} = \tfrac{A_n^* T_{n-}^2}{q}\int_{U_{c-}}^{\infty}\left(1+\tfrac{E_x}{kT_{n-}}\right)e^{h_c - E_x/kT_{n-}}dE_x \quad (85)$$

The corresponding integral using Fermi-Dirac statistics is (see Derivation 4 in Appendix G):

$$\mathbf{S}_{n-\rightarrow+}^{therm} = \frac{A_n^* T_{n-}^2}{q} \int_{U_{c-}}^{\infty} \left\{ \begin{array}{r} \left(h_c - \ln\left(1+e^{h_c - E_x/kT_{n-}}\right)\right)\ln\left(1+e^{h_c - E_x/kT_{n-}}\right) + \mathrm{Li}_2\left(\frac{1}{1+e^{E_x/kT_{n-} - h_c}}\right) \\ + \ln\left(\frac{1}{1+e^{E_x/kT_{n-} - h_c}}\right)\ln\left(\frac{1}{1+e^{h_c - E_x/kT_{n-}}}\right) \end{array} \right\} dE_x \quad (86)$$

where again $\mathrm{Li}_2(x)$ is the dilogarithm function (see Appendix H). Similar integrals apply for the tunneling energy flux except for the use of the transmission probability and the different limits of integration. Figure 14 plots the normalized energy flux versus energy for the barrier shown in Figure 4. Again, the Boltzmann expression approximates the Fermi-Dirac expression at higher energies.

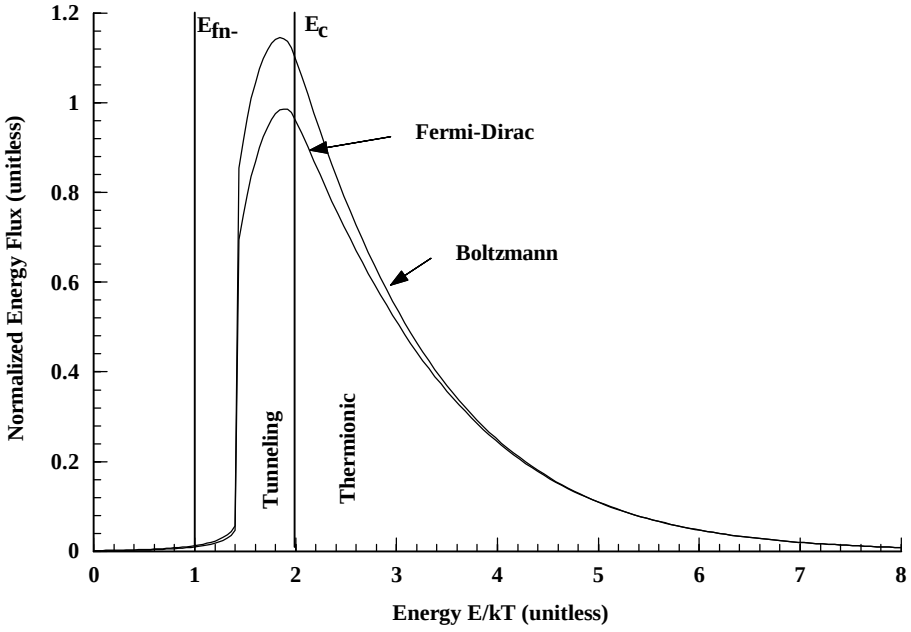

Figure 14 - Kinetic energy flux versus energy for the barrier in Figure 4

Because of the transmission probability, SimWindows calculates the tunneling integral numerically. There does exist analytical solutions for the thermionic emission energy flux using both Boltzmann and Fermi-Dirac statistics (see Derivations 3 and 4 in Appendix G). The Boltzmann result is:

$$\mathbf{S}_{n-\to+}^{therm} = \frac{A_n^* kT_{n-}^3}{q}\left(2 + \frac{U_{c-}}{kT_{n-}}\right)e^{h_{c-} - U_{c-}/kT_{n-}} \tag{87}$$

This expression can be written in terms of the Boltzmann thermionic emission current. This expression states that the kinetic energy carried by the electrons thermionically emitted over the barrier is 2kT plus the barrier height. This result is different than an "intuitive" result of 3/2kT plus the barrier height which would result if the energy flux were given by the average energy times the average velocity. Since the energy is actually given by (79) which is an "average energy velocity," equation (87) is the actual result for the carrier energy flux. The result using Fermi-Dirac statistics is:

$$\mathbf{S}_{n-\to+}^{therm} = \frac{A_n^* kT_{n-}^3}{q}\left[\begin{array}{l} 2\left\{\mathrm{Li}_3\left(\frac{1}{1+e^{U_{c-}/kT_{n-}-h_{c-}}}\right)+\mathrm{Li}_3\left(\frac{1}{1+e^{h_{c-}-U_{c-}/kT_{n-}}}\right)-\mathrm{Li}_3(1)\right\} \\ +\left(\frac{U_{c-}}{kT_{n-}}\right)\mathrm{Li}_2\left(\frac{1}{1+e^{U_{c-}/kT_{n-}-h_{c-}}}\right) \\ +\frac{1}{3}h_{c-}\left(h_{c-}^2+p^2\right)-\left(\frac{U_{c-}}{kT_{n-}}\right)\left(\frac{h_{c-}^2}{2}+\frac{p^2}{3}\right)+\frac{1}{6}\left(\frac{U_{c-}}{kT_{n-}}\right)^3 \\ -\ln\left(1+e^{U_{c-}/kT_{n-}-h_{c-}}\right)\left\{\begin{array}{l}\frac{2}{3}\ln^2\left(1+e^{U_{c-}/kT_{n-}-h_{c-}}\right) \\ -\left(\frac{3}{2}\frac{U_{c-}}{kT_{n-}}-h_{c-}\right)\ln\left(1+e^{U_{c-}/kT_{n-}-h_{c-}}\right) \\ +\left(\frac{U_{c-}}{kT_{n-}}\left(\frac{U_{c-}}{kT_{n-}}-h_{c-}\right)-\frac{p^2}{3}\right)\end{array}\right.\end{array}\right] \tag{88}$$

where Li_3 is the trilogarithm function (see Appendix H). The quantity in the bracket is unitless and only a function of the Planck potential, h_c, and the barrier height divided by the temperature, *U/kT*. Equation (88) reduces to (87) for Boltzmann statistics, since the first two terms in the bracket in (88) yields (87) and all other terms cancel out. Figure 15 shows that equation (88) approaches (87) for large barrier heights. This figure shows the normalized energy flux versus the barrier height for a quasi-fermi level 1 kT above the conduction band.

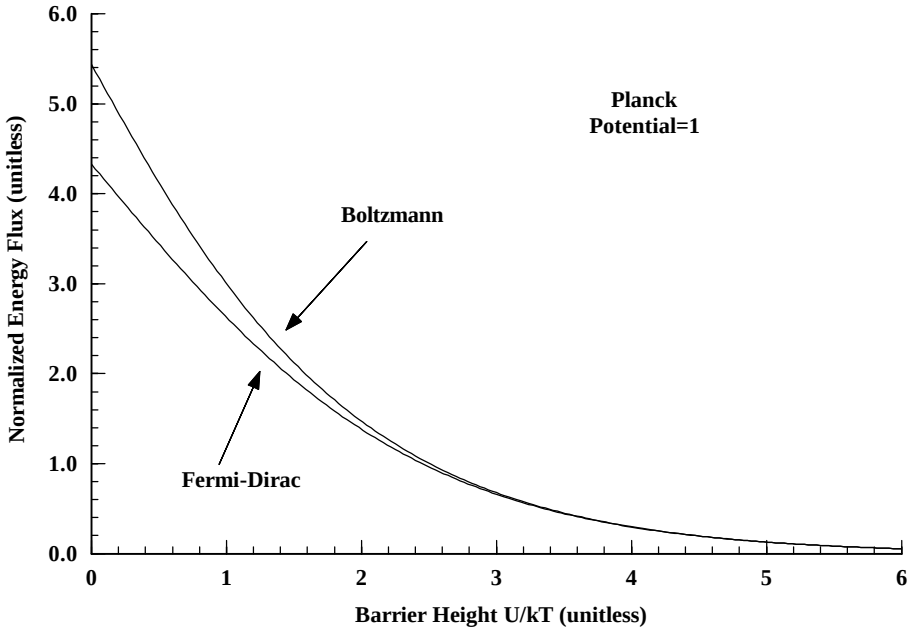

Figure 15 - Normalized thermionic emission energy flux

Figure 15 shows a difference compared with the thermionic emission expression for current shown in Figure 7. The error associated with using Boltzmann statistics for the energy flux is less than that for the current. In the thermionic emission expressions, the Boltzmann distribution results in an incorrect number of low energy electrons contributing to both current and energy flux. The effect on the current is greater since these low energy carriers have the same charge has the higher energy carriers, but the energy carried by the low energy carriers is less than the energy carried by the high energy carriers.

There are two items to note about equation (88). First, the complexity of (88) is partly due to manipulation that makes the arguments of the trilogarithm functions less than one. When the arguments are less than one, the trilogarithm functions can be evaluated using the summation presented in Appendix H. Second, it is possible to verify that the total energy flux (thermionic, tunneling, and potential) is zero when the

quasi-fermi level is constant across a barrier. This is a necessary requirement for any flux equation.

2.4.1.2.3 Lattice Energy Flux

SimWindows extends the model for the lattice energy flux to account for lateral energy loss of devices. Although SimWindows solves the semiconductor equations in one dimension, an extended model simulates energy flow out the sides of devices. It was necessary to devise an extended model since the temperature rise in simulated VCSEL structures was too high when using the standard one dimensional model. The extended lattice energy flux model is:

$$\mathbf{S}_{lat} = -k(x)\nabla T_L \hat{\mathbf{x}} + \frac{\Delta x}{pr_d^2} k_e(x)(T_L(x) - T_{env})\hat{\mathbf{r}} \tag{89}$$

where $k(x)$ is the thermal conductivity of the material, $k_e(x)$ is the effective thermal conductivity of the environment per unit length of the device, and r_d is the radius of the device. Both $k(x)$ and $k_e(x)$ are in units of W cm^{-1} K^{-1}. The first term is the standard lattice energy flux expression. The second term is the additional lateral energy flux that depends on the local lattice temperature and the environment temperature.

To calculate $k_e(x)$, SimWindows assumes that the device is a cylinder of radius r_d and is surrounded by a heat sink of radius r_e at a temperature of T_{env} as Figure 16 shows. For this geometry, there is an analytical solution for the temperature as a function of radius between the device and the environment. The equation for the temperature as a function of radius is:

$$T_{env}(x,r) = T_{env} - \frac{T_L(x) - T_{env}}{\ln\left(\frac{r_{env}}{r_d}\right)} \ln\left(\frac{r}{r_d}\right) \tag{90}$$

The derivation for this equation starts by integrating the normal component of the heat flux on a circular path around the device. Integrating the result from the radius of the device to radius of the environment yields equation (90). Figure 17 plots this function for the cases where the internal device temperature is 300K and 500K. In both cases the external environment temperature is 400K, the radius of the device is 3.5 microns, and the radius of the environment is 100 microns.

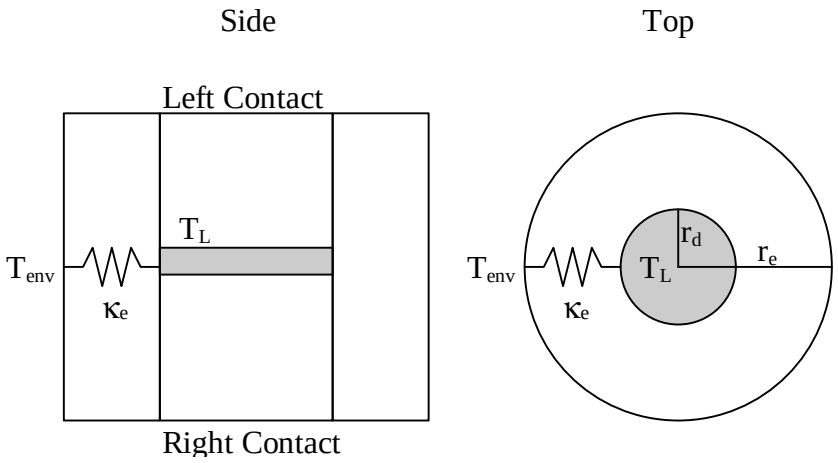

Figure 16 - Geometry for lateral heat flow

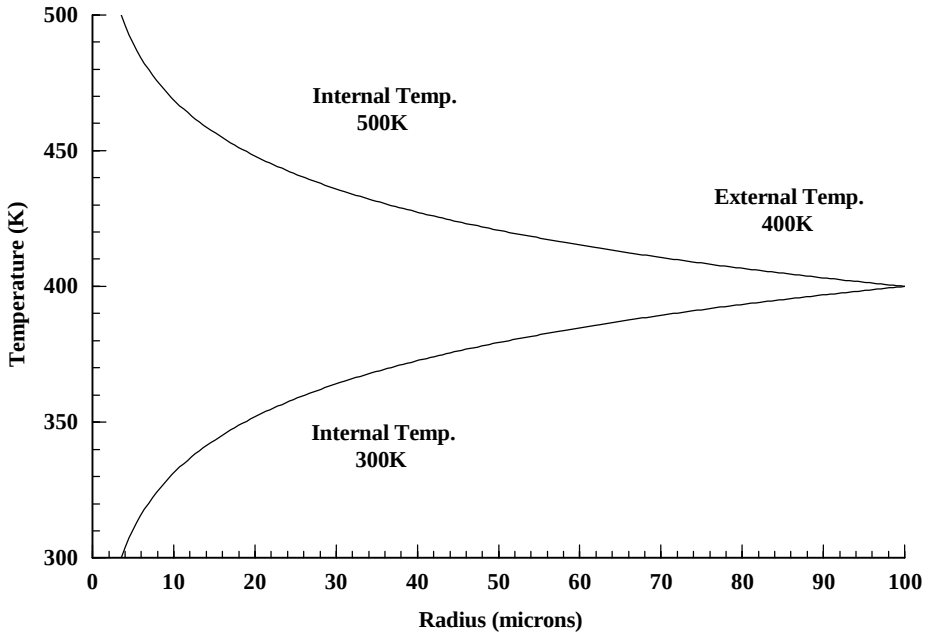

Figure 17 - Environment temperature versus radius

Equation (91) calculates the effective thermal conductivity between the device and the environment:

$$k_e(x, T_L(x), T_{env}) = \frac{2p}{\int_{r_d}^{r_e} \frac{dr}{r\,k(x,T(x,r))}} \tag{91}$$

Since k is temperature dependent, the derivations of (90) and (91) must use the temperature dependence of k. Since the user supplies a general function for k, (90) and (91) typically do not have analytical solutions. For typical semiconductor materials, there is a solution to this problem without numerically evaluating (90) and (91). By assuming that k is temperature independent, (91) yields:

$$k_e(x, T_L(x), T_{env}) = k(x)\frac{2p}{\ln\left(\frac{r_e}{r_d}\right)} \tag{92}$$

Now use the temperature dependence of k to evaluate (92). One approach would be to

assume that k_e depends only on the internal lattice temperature. A second approach would be to assume that k_e depends on the average of the internal lattice temperature and external environment temperature. These two approaches yield the following relations:

$$k_e(x, T_L(x), T_{env}) = k\left(x, T_L(x)\right)\frac{2p}{\ln\left(\frac{r_e}{r_d}\right)}$$
$$k_e(x, T_L(x), T_{env}) = k\left(x, \frac{T_L(x)+T_{env}}{2}\right)\frac{2p}{\ln\left(\frac{r_e}{r_d}\right)} \quad (93)$$

Figure 18 plots k_e versus the internal lattice temperature using the two relations in (93). It also plots the numerical calculation of (91). This figure uses the temperature dependence of GaAs outlined in section 2.6. It is obvious that assuming k_e varies with the average of the internal and environment temperatures is quite reasonable. For the internal temperature range used in Figure 18, the error between the numerical and approximate results was less than 0.1%. It is also clear from Figure 18 that simply using the internal temperature to control k_e is not adequate. Note that the results using the average temperature, the internal device temperature, and the numerical evaluation are identical when the internal temperature is the same as the external temperature. In this case the thermal conductivity from the device to the environment is constant.

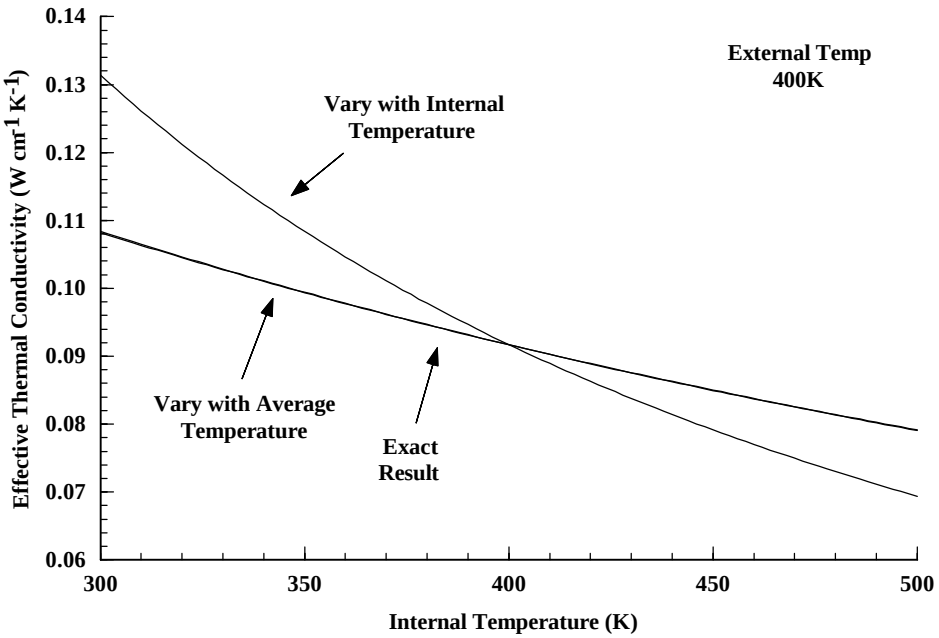

Figure 18 - Effective thermal conductivities versus internal temperature

2.4.1.3 Recombination/Generation

To complete the three temperature model, the energy flux must balance the energy change due to carrier recombination and energy relaxation. The energy rate equations, (74) through (76), use the sum of all the energy loss mechanisms. The expressions for the total energy loss are:

$$W_n^{tot} = W_{n,shr}^{tot} + W_{n,b-b}^{tot} + W_{n,stim}^{tot} - W_{n,opt}^{tot} + W_{n,relax} \tag{94}$$

$$W_p^{tot} = W_{p,shr}^{tot} + W_{p,b-b}^{tot} + W_{p,stim}^{tot} - W_{p,opt}^{tot} + W_{p,relax} \tag{95}$$

$$W_{lat}^{tot} = W_{n,shr}^{tot} + W_{p,shr}^{tot} + W_{n,relax} + W_{p,relax} \tag{96}$$

Equations (94) and (95) express the total carrier energy loss as the sum of the energy loss from SHR recombination, spontaneous emission, stimulated emission, external optical generation, and the carrier energy relaxation. These equations assume that there is no direct energy transfer between electrons and holes. Equation (96) expresses

that only certain energy loss mechanisms from the carriers contribute to the lattice energy. Since spontaneous emission, stimulated emission, and external generation add or remove energy from photons, the only energy terms that interact with the lattice are SHR recombination and carrier energy relaxation. Equations (94) through (96) are similar to the energy loss expressions used in [17] except for the addition of the photon generation and absorption terms. Reference [17] also includes energy change from impact ionization and Auger recombination which SimWindows does not model.

Since most of the energy loss terms in (94) through (96) depend on the total energy density of the carriers, it is convenient to first present the expressions for the total energy density. The derivation for these relations is similar to the derivation for the carrier concentrations. For bulk materials, the energy density for electrons and holes is:

$$u_n = n\left(\tfrac{3}{2}kT_n\frac{F_{3/2}(h_c)}{F_{1/2}(h_c)} + E_c\right) \qquad u_p = p\left(\tfrac{3}{2}kT_p\frac{F_{3/2}(h_v)}{F_{1/2}(h_v)} - E_v\right) \tag{97}$$

The energy density for electrons and holes in quantum wells is:

$$u_{n,2d} = n_{2d}\left(kT_n\frac{F_1\left(h_c-\frac{E_{nqw}}{kT_n}\right)}{F_0\left(h_c-\frac{E_{nqw}}{kT_n}\right)} + E_{nqw} + E_c\right) \quad u_{p,2d} = p_{2d}\left(kT_p\frac{F_1\left(h_v-\frac{E_{pqw}}{kT_p}\right)}{F_0\left(h_v-\frac{E_{pqw}}{kT_p}\right)} + E_{pqw} - E_v\right) \tag{98}$$

$$u_n(x) = \left|y_n(x)\right|^2 u_{n,2d} \qquad u_p(x) = \left|y_p(x)\right|^2 u_{p,2d} \tag{99}$$

These energy densities represent the kinetic plus potential energies which is consistent with the previous definitions of the energy flux and the energy rate equations.

The average energy of the carriers is just the total energy divided by the number of carriers. From (97) through (99), the average energy is 3/2 kT plus the band edge for bulk materials and 2/2 kT plus the quantized energy level plus the band

edge for quantum wells. This follows the concept that there is 1/2 kT of kinetic energy for each degree of freedom for the carrier.

The energy loss terms can now use the relations for the total energy density of the carriers. For carriers in bulk materials, the energy loss due to each process is:

$$W_{n,shr}^{tot} = \left(\frac{u_n}{n}\right)U_{shr} \qquad W_{p,shr}^{tot} = \left(\frac{u_p}{p}\right)U_{shr} \tag{100}$$

$$W_{n,b-b}^{tot} = \left(\frac{u_n}{n}\right)U_{b-b} \qquad W_{p,b-b}^{tot} = \left(\frac{u_p}{p}\right)U_{b-b} \tag{101}$$

$$W_{n,stim}^{tot} = E_{n,stim}U_{stim} \qquad W_{p,stim}^{tot} = E_{p,stim}U_{stim} \tag{102}$$

$$\begin{aligned} W_{n,opt}^{tot} &= \sum_{hu_{opt}}\left(\frac{m_p^*}{m_n^*+m_p^*}(hu_{opt}-E_g)G_{u,opt}\right)+E_cG_{opt} \\ W_{p,opt}^{tot} &= \sum_{hu_{opt}}\left(\frac{m_n^*}{m_n^*+m_p^*}(hu_{opt}-E_g)G_{u,opt}\right)-E_vG_{opt} \end{aligned} \tag{103}$$

$$W_{n,relax} = \frac{u_n(T_n)-u_n(T_{lat})}{t_{wn}} \qquad W_{p,relax} = \frac{u_p(T_p)-u_p(T_{lat})}{t_{wp}} \tag{104}$$

The influence of quantum wells modifies only equation (103). The corresponding equations for quantum wells are:

$$\begin{aligned} W_{n,opt}^{tot} &= \sum_{hu_{opt}}\left(\frac{m_p^*}{m_n^*+m_p^*}(hu_{opt}-E_{gqw})G_{u,opt}\right)+(E_{nqw}+E_c)G_{opt} \\ W_{p,opt}^{tot} &= \sum_{hu_{opt}}\left(\frac{m_n^*}{m_n^*+m_p^*}(hu_{opt}-E_{gqw})G_{u,opt}\right)+(E_{pqw}-E_v)G_{opt} \end{aligned} \tag{105}$$

Various assumptions are inherent in these equations for the energy loss. The expressions for both SHR and spontaneous recombination assumes that on average, the recombination event removes an electron with an average energy. For stimulated emission, the recombination event removes an electron at the energy dictated by the

photon energy. This is also true of external optical generation where the photon energy determines the energy of the generated electron and hole. The energy relaxation process assumes that there is a lifetime for the carriers to relax from their present energy density to an energy density that is in equilibrium with the lattice.

2.4.1.4 Boundary Conditions

The boundary conditions for the three temperature model are somewhat different than the boundary conditions for the electrical equations. In the case of electron and hole temperatures, SimWindows assumes that there is an infinite energy relaxation rate at the contact. This implies that the electron and hole temperatures are equal to the lattice temperatures at the contact:

$$T_n(0) = T_L(0) \qquad T_n(L) = T_L(L) \tag{106}$$

$$T_p(0) = T_L(0) \qquad T_p(L) = T_L(L) \tag{107}$$

The boundary condition for the lattice temperature is more complex. SimWindows uses general boundary conditions where specified effective thermal conductivities and specified external heat sink temperatures control the energy fluxes at the contacts. The expressions for the contact energy fluxes are:

$$\mathbf{S}_{lat}(0) = -k_l(T_L(0) - T_l) \qquad \mathbf{S}_{lat}(L) = k_r(T_L(L) - T_r) \tag{108}$$

where k_l and k_r are the specified effective thermal conductivities of the left and right surfaces and T_l and T_r are the specified temperatures of the left and right heat sinks, respectively. These relations join the device to ideal heat sinks through effective thermal conductivities. By using equation (89) for the lattice energy flux and assuming that the lateral energy flux is zero at the contact, the relations in (108) yield:

$$-k(0)\nabla T_L\big|_{x=0} + k_l T_L(0) = k_l T_l$$
$$k(L)\nabla T_L\big|_{x=L} + k_r T_L(L) = k_r T_r \qquad (109)$$

These show that the boundary condition is actually a mixed boundary condition involving both the temperature and the derivative of the temperature at the contact. There are two limiting cases for this boundary condition. In the case where k_l or k_r is infinite, the contact is an ideal heat sink and the contact temperature will be equal to the heat sink temperature. In the case were k_l or k_r is zero, the contact is an ideal insulator with no energy flux and the derivative of the temperature at the contact will be zero.

With the equations for the energy flux, the energy loss, and the boundary conditions, it is possible to solve for the three temperatures using the rate equations (74) through (76). SimWindows does not presently implement this model. Two simplifying assumptions result in two independent models that SimWindows does implement: the "Single Temperature Model" and the "Hot Electron Model."

2.4.2 Single Temperature Model

The first assumption in the Single Temperature Model is that the energy exchange between the electrons, holes, and lattice is instantaneous. This forces the electrons, holes and lattice to be in equilibrium with each other, and one temperature describes the average energy of all the particles in each system. This model treats the electrons, holes, and lattice as one system described by a single temperature. However, the three systems are out of equilibrium with the environment and the temperature of the electrons, holes, and lattice still varies within the device.

The same equations described for the three temperature model still model the

combined system of electrons, holes, and lattice. The key difference is that the rate equation for the combined system is just the sum of the rate equations for the three independent systems. In steady state, adding equations (74) through (76) yield:

$$\nabla \bullet (\mathbf{S}_{lat}(x) + \mathbf{S}_n(x) + \mathbf{S}_p(x)) + W_n^{tot} + W_p^{tot} - W_{lat}^{tot} = 0 \tag{110}$$

Adding equations (94) and (95) and subtracting equation (96) yields the total energy loss expression:

$$W_n^{tot} + W_p^{tot} - W_{lat}^{tot} = \left(\tfrac{3}{2} kT_n \frac{F_{3/2}(h_c)}{F_{1/2}(h_c)} + \tfrac{3}{2} kT_p \frac{F_{3/2}(h_v)}{F_{1/2}(h_v)} + E_g\right) U_{b-b} + h\nu_{stim} U_{stim} - h\nu_{opt} G_{opt} \tag{111}$$

For quantum wells, the corresponding equation is:

$$W_n^{tot} + W_p^{tot} - W_{lat}^{tot} = \left(kT_n \frac{F_1\left(h_c - \frac{E_{nqw}}{kT_n}\right)}{F_0\left(h_c - \frac{E_{nqw}}{kT_n}\right)} + kT_p \frac{F_1\left(h_v - \frac{E_{pqw}}{kT_p}\right)}{F_0\left(h_v - \frac{E_{pqw}}{kT_p}\right)} + E_{gqw} \right) U_{b-b} + h\nu_{stim} U_{stim} - h\nu_{opt} G_{opt} \tag{112}$$

These results make physical sense. Since the electrons, holes, and lattice are now one system, the system can only lose or gain energy through the generation or absorption of photons. Each of the terms on the right hand side of equations (111) and (112) represents energy loss or gain through interaction with photons.

2.4.3 Hot Electron Model

The second assumption is that the energy exchange between the electron population and the other two systems is not fast enough to keep the electrons in thermal equilibrium, but that the holes and lattice are in equilibrium with the environment. The electron temperature can vary within the device, but the hole and lattice temperatures are still at the environment temperature. The lattice and the holes act as an infinite reservoir where the temperature remains constant. In this case,

SimWindows uses the electron energy flux and energy loss expressions to solve the energy rate equation, (74).

2.5 Quantum Well Issues

Quantum wells are an important feature which SimWindows model. They allow SimWindows to model many kinds of optoelectronic devices based on quantum wells, and it was desirable to incorporate quantum wells in a manner consistent with the standard drift diffusion model. This chapter detailed the influence on the standard equations from quantum wells. This section will address the limitations of the quantum well model as a whole and explain the necessary features for a more advanced quantum well model. Table 3 lists the various required features to simulate quantum wells and how SimWindows implements those features.Table 3 also lists how a more general model would implement the same required features.

Table 3 - Comparison between SimWindows treatment and general treatment of quantum wells.

Feature	SimWindows	General
Energy Levels	Single Level Finite Well	Multiple Levels Schrödinger's Equation
Wavefunctions	Infinite Well	Schrödinger's Equation
Charge	2D, 3D Density of States	2D, 3D Density of States
Current	Thermionic Emission	Thermionic Emission Tunneling
Recombination Rate	1st electron to 1st hole Overlap integral	All allowed transitions Overlap integral
Index of Refraction Absorption	analogous to bulk expressions	Computed

SimWindows calculates the quantum well energy levels using analytical expressions for the finite height quantum well. It also only uses the lowest electron and hole levels. This is a reasonable approximation for the electrons since usually only one and at most two levels are present for the typical size (80-100Å) quantum wells used by devices presented later. This is a less reasonable approximation for holes since both light and heavy hole levels are present. A second consequence of using the finite well approximation, is that SimWindows can not modify the quantized energy levels with an application of an external field. SimWindows maintains the same energy level relative to the band edge at the middle of the well. To a first order this is a good approximation for low fields and applicable to the devices presented here that are operated at either zero or forward bias.

The infinite well approximation for the wavefunctions is reasonable again because the devices here are operated at either zero or forward bias. This approximation ignores the penetration of the carrier wavefunctions into the barriers, but the amount of penetration is the smallest for the lowest quantized energy levels. Because of these approximations, SimWindows is not able to model devices such as the self electro-optic effect device (SEED) which controls the overlap of electron and hole wavefunctions through the use of an external electric field [32]. The overlap integral between the electron and hole wavefunctions will always be one, but SimWindows is ready to use different wavefunctions in the future. A more complete and accurate quantum well model is to solve Schrödinger's equation numerically using the conduction and valence band edges generated by Poisson's equation [33]. This would allow SimWindows to simulate devices such as the SEED.

SimWindows treats the current into and out of quantum wells using thermionic emission current expressions. This is suitable when multiple quantum wells are spaced far enough apart that tunneling can be neglected. Devices that incorporate superlattices would require a solution to Schrödinger's equation to calculate the minibands and the tunneling probability between quantum wells.

Since SimWindows uses the lowest electron and hole quantized energy levels, the spontaneous and SHR recombination rates in the quantum well is between these two states. SimWindows also uses expressions for these recombination rates that are similar to bulk expressions. A more accurate method is to use a quantum mechanical approach to calculate the transition rate between each electron and hole sublevel. The total recombination rate would be the sum of the recombination rates between every combination of electron and hole sublevels [27,34].

The index of refraction and the absorption of quantum wells are by default based on the results for bulk material. Since users specify these parameters, they can be chosen to be any value. A more accurate approach would involve computing the matrix elements associated with band-to-band transitions as well as excitonic transitions. These calculations can yield the absorption and refractive index of arbitrarily shaped quantum wells [35].

SimWindows also does not model other effects such as band gap narrowing with carrier concentration. Despite the limitations described in this section, the quantum well model is sufficient for the device examples presented in the next chapter. Future work could include expanding the quantum well model and incorporating a Schrödinger's equation solver into SimWindows. Although integrating a Schrödinger's

equation solver would require work, the flexibility of SimWindows makes the task easier.

2.6 Material Models

The mathematical model described in this chapter is a function of many different material and device constants. The user must specify a value for every constant to solve uniquely the semiconductor equations. In SimWindows, there are three distinct locations where the user can specify these constants: the material parameters file, the device file, and from within the user interface itself. Table 4 lists all specified variables, their definition, units, and where to specify the variable in the program. By the design of SimWindows, any variable in the device file will override the value in the material parameters file.

SimWindows includes a default material parameters file that contains material parameters for Si and $Al_xGa_{1-x}As$. Many of the material parameters are themselves functions of other variables. Table 5 shows the default models for each of the material parameters for Silicon. Table 6 shows the corresponding models for $Al_xGa_{1-x}As$. SimWindows provides the user with the flexibility to change any of the models for any of the material parameters in Table 5 and Table 6. This includes not only changing constants, but also changing the functional dependence of material parameters.

Table 4 - Specified variables: M - Materials file, D - Device file, S - SimWindows

Symbol	Definition	Units	Location
A_c	Laser cavity area	m^2	D
B	Spontaneous recombination constant	$cm^3\ s^{-1}$	M,D
B_{qw}	QW spontaneous recombination constant	$cm^2\ s^{-1}$	M,D
E_D,E_A	Donor and acceptor energy levels	eV	D
E_g	Bulk band gap	eV	M,D
g_D,g_A	Donor and acceptor degeneracy factors	unitless	D
L	Length of device	m	D
L_c	Length of the laser cavity	m	D,S
L_{qw}	Length of quantum well	m	D
m_{cn}^*,m_{cp}^*	Electron and hole conductivity masses	kg	M,D
m_n^*,m_p^*	Electron and hole DOS masses	kg	M,D
n_{real}	Real part of the refractive index	unitless	M,D
N_D,N_A	Donor and acceptor concentrations	cm^{-3}	D
R_l,R_r	Left and right mirror reflectivities	unitless	D,S
r_d	Device radius	m	D
r_e	Environment radius	m	S
T_{env}	Environment temperature	K	S
T_l, T_r	Left and right surface temperatures	K	S
V_l, V_r	Left and right contact voltages	V	S
x	Device position	m	D
a	Absorption coefficient	cm^{-1}	M,D
a_s	Scatting losses in the laser cavity	cm^{-1}	S
b	Fraction of spontaneous emitted photons emitted into lasing mode.	unitless	S
$\in$	Dielectric permitivity	$F\ cm^{-1}$	M,D
k	Thermal conductivity	$J\ s^{-1}\ cm^{-1}\ K^{-1}$	M,D
dk/dT	Derivative of thermal conductivity wrt. temperature	$J\ s^{-1}\ cm^{-1}\ K^{-2}$	M,D
k_l, k_r	Left and right surface thermal conductivities	$J\ s^{-1}\ cm^{-2}\ K^{-1}$	S
m_n , m_p	Electron and hole mobilities	$cm^2\ V^{-1}\ s^{-1}$	M,D
u_n,u_n	Energy power dependence of the electron and hole momentum relaxation times	unitless	M,D
u_{opt}	External optical generation frequency	s^{-1}	S
t_n, t_n	Electron and hole SHR recombination lifetime	s	M,D
t_{wn}, t_{wn}	Electron and hole relaxation lifetime	s	M,D
c	Electron affinity	eV	M,D

Table 5 - Silicon material parameters

Symbol	Model	Ref.
B	1.5×10^{-10}	NA
B_{qw}	0	NA
E_g	$1.124 - 4.73x10^{-4}\left(\frac{T_{lat}^2}{636+T_{lat}} - \frac{300^2}{636+300}\right)$	[44]
m_{cn}^*	0.26	[43]
m_{cp}^*	0.386	[43]
m_n^*	1.08	[43]
m_p^*	0.81	[43]
n_{real}	3.44	[43]
a	$0 < E_{opt} \le 1.1 \quad 0$ $1.1 < E_{opt} \le 2.5 \quad 6x10^3\left(E_{opt}-1.1\right)^2$ $2.5 < E_{opt} \le 3.2 \quad \left\{\begin{matrix}6x10^3\left(E_{opt}-1.1\right)^2 \\ +8x10^4\left(E_{opt}-2.5\right)^2\end{matrix}\right\}$ $3.2 < E_{opt} \quad \left\{\begin{matrix}6x10^3\left(E_{opt}-1.1\right)^2 \\ +8x10^4\left(E_{opt}-2.5\right)^2 \\ +1.26x10^6\left(E_{opt}-3.2\right)^{0.5}\end{matrix}\right\}$	Note 1
$\in$	11.7	[43]
k	1.412	[43]
dk/dT_{lat}	0	Note 2
m_n	$88\left(\frac{T_n}{300}\right)^{-0.57} + 7.4x10^8\left(\frac{T_n^{-2.33}}{1+\left(\frac{N_D+N_A}{1.432x10^{17}}\right)\left(\frac{T_n}{300}\right)^{-2.546}}\right)$	[36]
m_p	$54.3\left(\frac{T_p}{300}\right)^{-0.57} + 1.36x10^8\left(\frac{T_p^{-2.33}}{1+\left(\frac{N_D+N_A}{2.671x10^{17}}\right)\left(\frac{T_p}{300}\right)^{-2.546}}\right)$	[36]
u_n	-0.5	Note 3
u_n	-0.5	Note 3
t_n	$1x10^{-7}$	NA
t_p	$1x10^{-7}$	NA
t_{wn}	$1x10^{-8}$	NA
t_{wp}	$1x10^{-8}$	NA
c	$1.124 + 2.365x10^{-4}\left(\frac{T_{lat}^2}{636+T_{lat}} - \frac{300^2}{636+300}\right)$	Note 4

Table 6 - Material parameters for $Al_xGa_{1-x}As$

Symbol	Model	Ref.
B	1.5×10^{-10}	NA
B_{qw}	1.54×10^{-4}	[39]
E_g	$0.0 < x \le 0.45 \quad 1.424 + 1.247x - 5.405x10^{-4}\left(\frac{T_{lat}^2}{204+T_{lat}} - \frac{300^2}{204+300}\right)$ $0.45 < x \le 1.00 \quad 1.9 + 0.125x + 0.125x^2 - 5.405x10^{-4}\left(\frac{T_{lat}^2}{204+T_{lat}} - \frac{300^2}{204+300}\right)$	[44]
m_{cn}^*	$0.0 < x \le 0.45 \quad 0.067 + 0.083x$ $0.45 < x \le 1.00 \quad 0.32 - 0.06x$	[40]
m_{cp}^*	$0.62+0.14x$	[40]
m_n^*	$0.067+0.083x$ $0.85-0.14x$	[40]
m_p^*	$0.62+0.14x$	[40]
n_{real}	"Oscillator Model"	[37,38] Note 5
a	$0 < E_{opt} \le E_g + 0.00087 \quad \exp(71(E_{opt} - E_g - 0.104))$ $E_g + 0.00087 < E_{opt} \quad 3.54x10^4\left(E_{opt} - E_g\right)^{0.5}$	[41]
$\in$	$13.18-3.12x$	[40]
k	$\frac{549.356}{1+12.7x-13.22x^2} T_{lat}^{-1.25}$	[42]
dk/dT_{lat}	$\frac{-686.695}{1+12.7x-13.22x^2} T_{lat}^{-2.25}$	Note 2
m_n	$0.0 < x \le 0.45 \quad 8000 - 22000x + 10000x^2$ $0.45 < x \le 1.00 \quad -255 + 1160x - 720x^2$	[40]
m_p	$370-970x+740x^2$	[40]
u_n	0.5	Note 6
u_n	0.5	Note 6
t_n	$1x10^{-8}$	NA
t_p	$1x10^{-8}$	NA
t_{wn}	$1x10^{-12}$	NA
t_{wp}	$1x10^{-12}$	NA
c	$0.0 < x \le 0.45 \quad 4.07 - 0.7482x + 2.702x10^{-4}\left(\frac{T_{lat}^2}{204+T_{lat}} - \frac{300^2}{204+300}\right)$ $0.45 < x \le 1.00 \quad 3.594 + 0.3738x - 0.143x^2 + 2.702x10^{-4}\left(\frac{T_{lat}^2}{204+T_{lat}} - \frac{300^2}{204+300}\right)$	Note 7

Notes on material parameters:

1. Analytical fit to data presented in [43].
2. This is the analytical derivative of the thermal conductivity with respect to the lattice temperature.
3. Factors correspond to acoustic phonon scattering.
4. Expression assumes that half of the band gap narrowing due to temperature contributes to the increase in electron affinity.
5. The "Oscillator Model" is a summation of nine independent oscillator models presented in [37] that approximates data presented in [38].
6. Factors correspond to optical phonon scattering.
7. Expressions yield conduction and valence band discontinuities that are presented in [40]. Expressions also assume that half of the band gap narrowing due to temperature contributes to the increase in the electron affinity.